Numer. Math. Theor. Meth. Appl.
doi: 10.4208/nmtma.OA-2023-0082

Vol. **xx**, No. x, pp. 1-40
x 2023

On Lagrange-Projection Schemes for Shallow Water Flows Over Movable Bottom with Suspended and Bedload Transport

Alessia Del Grosso[1,*], Manuel J. Castro Díaz[2], Christophe Chalons[1] and Tomás Morales de Luna[2]

[1] *Université Paris-Saclay, UVSQ, CNRS, Laboratoire de Mathématiques de Versailles, 78000, Versailles, France*
[2] *Dpto. de Análisis Matemático, Facultad de Ciencias, Universidad de Málaga, Campus de Teatinos S/N, 29081 Málaga, Spain*

Received 5 July 2023; Accepted (in revised version) 10 July 2023

Abstract. In the present work we aim to simulate shallow water flows over movable bottom with suspended and bedload transport. In order to numerically approximate such a system, we proceed step by step. We start by considering shallow water equations with non-constant density of the mixture water-sediment. Then, the Exner equation is included to take into account bedload sediment transport. Finally, source terms for friction, erosion and deposition processes are considered. Indeed, observe that the sediment particle could go in suspension into the water or being deposited on the bottom. For the numerical scheme, we rely on well-balanced Lagrange-projection methods. In particular, since sediment transport is generally a slow process, we aim to develop semi-implicit schemes in order to obtain fast simulations. The Lagrange-projection splitting is well-suited for such a purpose as it entails a decomposition of the (fast) acoustic waves and the (slow) material waves of the model. Hence, in subsonic regimes, an implicit approximation of the acoustic equations allows us to neglect the corresponding CFL condition and to obtain fast numerical schemes with large time step.

AMS subject classifications: 65M08, 76M12, 35L60
Key words: Shallow water flows, movable bottom, erosion-deposition processes, Lagrange-projection schemes, implicit-explicit schemes.

1. Introduction and mathematical model

Sediment transport is an interesting and active topic in the field of geophysical flows. Sediment is transported by the action of a river current or due to currents near

*Corresponding author. *Email addresses:* alessia.del-grosso2@uvsq.fr (A. Del Grosso), mjcastro@uma.es (M. Castro Díaz) christophe.chalons@uvsq.fr (C. Chalons), tmorales@uma.es (T. Morales de Luna)

coastal areas mainly in two ways: a suspended load (fine fractions carried by the flow) and bedload (coarse fractions which move close to the bottom rolling, jumping and sliding), see [54].

Knowledge of sediment transport has different practical applications. For instance, in civil engineering, to plan the extended life of a dam forming a reservoir. Moreover, sediment deposition downstream reduces river capacity in that area, which may be a potential problem in flood situations. Sediments also play an important role in some environmental problems as well. For example, suspended sediments have a direct impact on fish habitat in river or estuaries [39].

A first common approach to model sediment transport by a fluid is to couple the shallow water equations [2, 45, 47] with the so-called Exner equation [30]. Many works have been proposed to study such a problem, which depends on an empirical definition of the solid transport flux for bedload transport (see [10,11,29,40,46,50,52] among many others). This first approach is then completed by including some transport equations for suspended sediment, that is sediment particles which have been eroded from the bottom and remain floating in the current for some time until subsequent sedimentation are sedimented afterwards (see [25,39,41,43,44,49,51] among many others).

One of the key points of such problems is that the characteristic times associated to sediment transport dynamics is much larger than the one corresponding to fluids. Hence, studying sediment transport usually requires long time simulations to see sediment's evolution. As such, numerical simulations will run for long wall-clock times, which are carried out in small time steps, mainly dominated by the characteristic fluid speed.

To overcome this difficulty, different strategies have been proposed. The most common approach is to use semi-implicit schemes (see [13–16] among others). In particular, this approach is used in [7,35], where bedload transport with the simple Grass formula is considered as well as variable density. Moreover, in [36], the authors propose a semi-implicit scheme based on the theta method for sediment bedload transport models with gravitational effects under subcritical regimes. Another approach is the use of the Lagrange-Projection strategy (see [12,20–22,28,48] and references therein). This framework allows us to naturally decouple the acoustic terms of the model from the transport ones. Such a decomposition is useful and very efficient to deal with subsonic or near low-Froude number flows. In such cases, the usual CFL time step limitation of Godunov-type schemes is driven by the acoustic waves and can thus be very restrictive. The Lagrange-projection strategy allows us to design a very natural implicit-explicit and large time step scheme, with a CFL restriction based on the (slow) transport waves and not on the (fast) acoustic waves. Therefore, in this paper, we consider the Lagrange-projection technique adapted to the problem of sediment transport. In particular, we aim to define a semi-implicit scheme for sediment transport problems.

Hence, let us briefly present the corresponding mathematical model. It is deduced from the Navier-Stokes equations under the hypothesis that the horizontal scale is much greater than the vertical one, assuming hydrostatic pressure and incompressibility of

the fluid. For more details about its derivation, we directly refer to [39]. As such, the system is composed of four equations, which express the evolution in time of the variables $h(x,t) \geq 0$, $h\rho(x,t) \geq 0$, $h\rho u(x,t)$ and $z(x,t)$. Here h and u stand respectively for the height and averaged velocity of the water over the bottom, whose elevation is represented by z. Then, ρ is the density of the mixture water-sediments, where the latter are transported by the currents and can either move along the bottom (bed-load) or being finer fractions carried by the flow (suspended-load). Finally, using $t > 0$ and x to represent the time and the axial coordinate respectively, the resulting model reads

$$\begin{cases} \partial_t h + \partial_x(hu) = \zeta\phi_z, & \text{(1.1a)} \\ \partial_t(h\rho) + \partial_x(h\rho u) = \zeta\phi_z\rho_z, & \text{(1.1b)} \\ \partial_t(h\rho u) + \partial_x(h\rho u^2 + p) + gh\rho\partial_x z = \rho_z\dfrac{u}{2}\zeta\phi_z - \tau_f(u), & \text{(1.1c)} \\ \partial_t z + \zeta\partial_x q_z = -\zeta\phi_z. & \text{(1.1d)} \end{cases}$$

In particular, in the third equation, the pressure term is given by $p = gh^2\rho/2$. Then, the evolution in time of the topography is described by the Exner equation, where $q_z = q_z(h, h\rho, h\rho u)$ represents the solid transport discharge. For the latter, there exist many different empirical laws for the solid transport discharge. Classically, it only depends on the hydrodynamical variables, $q_z = q_z(h,u)$, and on different parameters that are calibrated depending on the type of the considered sediments. Among many others, we refer for instance to the works [1, 3, 6, 9, 11, 50] for more information. For the sake of simplicity, here we only consider two of the most used formulations: the first one is the simplest one, namely the Grass model [40]. It expresses q_z as a power law of the velocity,

$$q_z = A_g u|u|^{m_g-1}, \quad m_g = 3 \tag{1.2}$$

with $A_g \in [0,1]$ a constant which represents the strength of the interaction between the sediment and the flow. Then, another (more realistic) possibility is given by the Meyer-Peter & Müller (MPM) formula [46], which reads

$$q_z = 8Q\,\mathrm{sign}(u)(\theta^* - \theta_c^*)_+^{3/2}, \quad \theta^* = \frac{u_*^2}{\mathrm{sgd}}, \quad u_*^2 = \frac{g\mu_f^2 u^2}{h^{1/3}}. \tag{1.3}$$

Moreover, $Q = d\sqrt{\mathrm{gsd}}$ is the characteristic discharge with $s = \rho_s/\rho_w - 1$ the relative density, ρ_s is the density of the sediment and ρ_w is the density of water. Finally, d represents the sediment diameter, μ_f is the dimensionless Manning's coefficient and θ_c^* is the critical Shield's stress for incipient motion. Let us observe that, depending on the particular form of q_z, the resulting system could be strictly hyperbolic or not. Indeed, we already know that the shallow water Exner system is strictly hyperbolic, with all real eigenvalues, in the case of Grass model (1.2). Then, regarding the MPM formula (1.3), it has been proved that a sufficient condition for the resulting model to be strictly hyperbolic is $|u| < 6gh$, which is generally true in physical situations, see [24, 39]. In any case, we underline that our numerical strategy can be applied whatever the formulation for q_z is.

Next, let us focus on the source terms. Here, $\phi_z = F_e - F_d$ expresses the sediment exchange between the bottom and the water-sediment mixture, where F_e and F_d are the erosion and deposition rate respectively. In particular, we state $F_e = v_s \mathcal{P} E_s$ where

$$v_s = \sqrt{\left(\frac{13.95\nu}{d}\right)^2 + 1.09\mathrm{sgd}} - \frac{13.95}{d}\nu$$

is the settling velocity of sediment where ν is the kinematic viscosity of the water and d is the sediment diameter. Then, the constant $\mathcal{P}$ stands for the volume fraction of the sediment in the bottom or, equivalently, $1 - \mathcal{P} = \Psi$ is the porosity of the bottom (see [38, 39]), with $\zeta = (1 - \Psi)^{-1}$. The value for the porosity of bed material is determined using the formulas described in [42, 56].

Subsequently, the sediment entrainment coefficient is given by

$$E_s = \frac{1.3 \times 10^{-7} \mathcal{Z}^5}{1 + 4.3 \times 10^{-7} \mathcal{Z}^5}, \quad \mathcal{Z} = \frac{\alpha_1 \sqrt{c_D}|u|}{v_s} \mathcal{R}_p^{\alpha_2}, \tag{1.4}$$

where $\mathcal{R}_p = \sqrt{\mathrm{sgd}}d/\nu$ is the Reynold number and c_D is bed drag coefficient. Finally, α_1, α_2 are two parameters depending on $\mathcal{R}_p$ and for which there exist different value choices. Here we refer to [39] and take

$$(\alpha_1, \alpha_2) = \begin{cases} (1, 0.6), & \text{if} \quad \mathcal{R}_p > 2.36, \\ (0.586, 1.23), & \text{if} \quad \mathcal{R}_p \leq 2.36. \end{cases}$$

Continuing with the deposition rate, we assume that $F_d = v_s c_z$, where c_z is the fractional concentration of suspension near the bed, namely,

$$c_z = c\left(0.4\left(\frac{d}{D_{sg}}\right)^{1.64} + 1.64\right),$$

where $c(x,t)$ is the volumetric sediment concentration such that

$$\rho(x,t) = \rho_w + c(x,t)(\rho_s - \rho_w)$$

and D_{sg} is the geometric mean size of the suspended sediment mixture. In particular, in this work we take $D_{sg} = d$ as all the particles are assumed to be of equal size. At last, $\rho_z = \rho_w \Psi + \rho_s(1 - \Psi)$ is the density of the saturated bottom.

Lastly and for the friction term, we state $\tau_f(u) = \rho u_*^2(1 + r_w)$ where r_w is the ratio of upper-interface resistance to bed resistance. For the sake of clarity, in Tables 1-1, we include the description of the parameters and symbols used in this work.

To complete the presentation of the mathematical model, let us observe that system (1.1) can be reformulated in compact form as follows:

$$\partial_t \mathbf{Q} + \partial_x \mathbf{F}(\mathbf{Q}) + \mathbf{B}(\mathbf{Q})\partial_x \mathbf{Q} = \mathbf{S}(\mathbf{Q}),$$

where $\mathbf{Q}$ is the vector of unknowns, $\mathbf{F}(\mathbf{Q})$ is the physical flux, $\mathbf{B}(\mathbf{Q})$ is the non-conservative product matrix and $\mathbf{S}(\mathbf{Q})$ is the source term. More explicitly,

$$\begin{aligned}
\mathbf{Q} &= \begin{pmatrix} h \\ h\rho \\ h\rho u \\ z \end{pmatrix}, \quad \mathbf{F}(\mathbf{Q}) = \begin{pmatrix} hu \\ h\rho u \\ h\rho u^2 + g\dfrac{h^2}{2}\rho \\ \zeta q_z \end{pmatrix}, \\
\mathbf{B}(\mathbf{Q}) &= \begin{pmatrix} 0 & 0 & 0 & 0 \\ 0 & 0 & 0 & 0 \\ 0 & 0 & 0 & gh\rho \\ 0 & 0 & 0 & 0 \end{pmatrix}, \quad \mathbf{S}(\mathbf{Q}) = \begin{pmatrix} \zeta\phi_z \\ \zeta\phi_z\rho_z \\ \rho_z\dfrac{u}{2}\zeta\phi_z - \tau_f(u) \\ -\zeta\phi_z \end{pmatrix}.
\end{aligned} \tag{1.5}$$

Then, let us recall that classic Saint Venant Exner system does not satisfy a global entropy equation. Nevertheless, as shown in [31], a modified version of Saint Venant Exner system could be introduced so that the model satisfies a global entropy. Therefore, we do not expect to find an entropy inequality for system (1.1), unless similar modifications are performed for Exner's equation, which is out of the scope of this paper. Nevertheless, we may prove a partial result which is given in the next theorem.

Theorem 1.1. *Consider system* (1.1) *without bedload transport, that is,* $q_z = 0$*. Then, smooth solutions of the system satisfy the following relation:*

$$\begin{aligned}
&\partial_t\left(\rho h\frac{u^2}{2} + \frac{g}{2}\rho h^2 + g\rho hz\right) \\
&\quad + \partial_x\left(\rho hu\left(\frac{u^2}{2}+\frac{g}{2}h\right) + up + g\rho huz\right) \\
&= \frac{g}{2}h\zeta\phi_z(\rho_z - \rho) + gz\zeta\phi_z\rho_z - u\tau_f.
\end{aligned}$$

Proof. Combining (1.1b) and (1.1c), we get

$$\partial_t u + \partial_x\frac{u^2}{2} + \frac{1}{\rho h}\partial_x p + g\partial_x z = -\frac{\rho_z}{\rho h}\zeta\phi_z\frac{u}{2} - \frac{1}{\rho h}\tau_f.$$

Multiplying this equation by ρhu and adding (1.1b) times $u^2/2$, we obtain

$$\partial_t\left(\rho h\frac{u^2}{2}\right) + \partial_x\left(\rho hu\frac{u^2}{2}\right) + u\partial_x p + g\rho hu\partial_x z = -u\tau_f. \tag{1.6}$$

Now, taking into account that $p = g\rho h^2/2$, from the Eq. (1.1a) we get

$$\partial_t h + u\partial_x h + \frac{p}{g\rho h/2}\partial_x u = \zeta\phi_z,$$

which, combined with (1.1b), gives

$$\partial_t\left(\frac{g}{2}\rho h^2\right) + \partial_x\left(\frac{g}{2}\rho h^2 u\right) + p\partial_x u = \frac{g}{2}h\zeta\phi_z(\rho + \rho_z). \tag{1.7}$$

Adding (1.6) and (1.7) gives us

$$\begin{aligned}&\partial_t\left(\rho h\frac{u^2}{2}+\frac{g}{2}\rho h^2\right)+\partial_x\left(\rho hu\left(\frac{u^2}{2}+\frac{g}{2}h\right)+up\right)+g\rho hu\partial_x z\\&=-u\tau_f+\frac{g}{2}h\zeta\phi_z(\rho+\rho_z).\end{aligned}$$

Finally, we have

$$\begin{aligned}g\rho hu\partial_x z&=g\rho hu\partial_x z+g\rho h(\partial_t z+\zeta\phi_z)+gz\big(\partial_t(\rho h)+\partial_x(\rho hu)-\zeta\phi_z\rho_z\big)\\&=\partial_t(g\rho hz)+\partial_x(g\rho huz)+g\rho h\zeta\phi_z-gz\zeta\phi_z\rho_z\end{aligned}$$

and the result follows. □

As a last remark and referring to [39], from a physical point of view it is interesting to consider the solutions of the model when $u=0$. Indeed, in this case the solution should satisfy

$$\begin{cases}\partial_t h=\zeta\phi_z,\\ \partial_t(h\rho)=\zeta\phi_z\rho_z,\\ \partial_x\left(\dfrac{gh^2\rho}{2}\right)=-gh\rho\partial_x z,\\ \partial_t z=-\zeta\phi_z.\end{cases}\tag{1.8}$$

Moreover, we observe that the free surface $H=h+z$ is constant in time but

$$\partial_x(h+z)=-\frac{h}{2\rho}\partial_x\rho,$$

and in particular

$$\partial_t\rho=\frac{\zeta\phi_z}{h}(\rho_s-\rho_w)(1-\Psi-c).$$

Thus, if $u=0$, we expect the free surface H to remain constant in time but the water height to decrease and the bed level to increase, as the sediments start to accumulate on the bottom. As a consequence, the density ρ will remain constant in time if $1-\Psi=c$, or either increase or decrease if $1-\Psi<c$ or $1-\Psi>c$ respectively.

The paper is organized as follows. To describe the numerical approach to approximate model (1.1), we will proceed step by step. We first consider a simplified version of the system with no source terms and constant bed level in time. The Lagrangian formulation of the resulting system is proposed. An approximate Riemann solver for the acoustic system is also described, see Section 2. Then, in Section 3, the strategy is extended in order to include the Exner equation. The numerical approximation is finally presented in Section 4, the source terms related to the friction and the erosion-deposition processes are considered as well. Section 5 is devoted to the numerical simulations while in Section 6 we draw the conclusions.

Table 1: Symbols with description and formula.

Symbol	Description	Value or formula
a	Parameter in syst. (2.12), (3.4)	$a \geq h^2\rho^2\bar{c}^2$
b	Parameter in syst. (3.4)	$u^2b^2 \geq (h\rho u)^2 + g(h\rho)^2\partial_u q_z$, $b > 0$
c	Volumetric sediment concentration	$c(x,t) = (\rho - \rho_w)(\rho_s - \rho_w)^{-1}$
$\bar{c}$	Sound speed	$\bar{c} = \sqrt{gh}$
c_D	Bed drag coefficient	-
c_z	Fractional concentration of suspension near by the bed	$c_z = c\big(0.4(d/D_{sg})^{1.64} + 1.64\big)$
d	Sediment diameter	[mm]
D_{sg}	Geometric mean size of the suspended sediment mixture	[mm]
E_s	Sediment entrainment coefficient	$E_s = (1.3 \times 10^{-7}\mathcal{Z}^5)/(1 + 4.3 \times 10^{-7}\mathcal{Z}^5)$
F_d	Deposition rate	$F_d = v_s c_z$
F_e	Erosion rate	$F_e = v_s\mathcal{P}E_s$
g	Gravitational acceleration	9.81 [m s^{-2}]
h	Water height	[m]
H	Free surface elevation	$H = h + z$
L	Volume ratio	$L(\xi,t) = \partial_\xi x(\xi,t)$
m	Mass variable	$\partial_x/(h_0\rho_0) = \partial_m$
p	Pressure term	$p = gh^2\rho/2$
$\mathcal{P}$	Volume fraction of the sediment in the bottom	$1 - \mathcal{P} = \Psi$
q_z	Solid transport discharge	-
Q	Characteristic discharge	$Q = d\sqrt{gsd}$
r_w	Ratio of upper-interface resistance to bed resistance	-
$\mathcal{R}_p$	Reynold number	$d\sqrt{gsd}/\nu$
s	Relative density	$s = \rho_s/\rho_w - 1$
t	Time	[s]
u	Averaged velocity of water	[m s^{-1}]
u_*^2	Bed shear velocity	$u_*^2 = g\mu_f^2 u^2/h^{1/3}$
v_s	Settling velocity of the sediment	$v_s = \sqrt{(13.95\nu/d)^2 + 1.09\mathrm{sgd}} - 13.95\nu/d$
x	Axial coordinate	-
z	Bed level	[m]
$\mathcal{Z}$	Parameter in Eq. (1.4)	$\mathcal{Z} = \alpha_1\sqrt{c_D}\lvert u\rvert\mathcal{R}_p^{\alpha_2}/v_s$
α_1	Parameter in Eq. (1.4)	1 if $\mathcal{R}_p > 2.36$, 0.6 otherwise
α_2	Parameter in Eq. (1.4)	0.586 if $\mathcal{R}_p > 2.36$, 1.23 otherwise
ζ	Parameter in model (1.1)	$\zeta = 1/(1 - \Psi)$
θ	Variable for the inverse of the density	$\theta = 1/\rho$
θ^*	Shield's parameter	$\theta^* = u_*^2/\mathrm{sgd}$
θ_c^*	Critical Shield's stress for incipient motion	-
λ	Relaxation parameter	-
μ_f	Dimensionless Manning's coefficient	[s m$^{-1/3}$]
ν	Kinematic viscosity of the water	1×10^{-6} [m s^{-2}]
ξ	Lagrangian coordinate	-

Table 1: Symbols with description and formula (cont'd).

Symbol	Description	Value or formula
Π	Relaxation linearization of $gh^2\rho/2$	-
ρ	Density of mixture of water and sediment	[g cm^{-3}]
ρ_w	Density of water	1 [g cm^{-3}]
ρ_s	Density of sediment	[g cm^{-3}]
ρ_z	Density of the saturated bottom	$\rho_z = \rho_w\Psi + \rho_s(1-\Psi)$
τ	Variable for the inverse of the water height	$\tau = 1/h$
τ_f	Friction term	$\tau_f(u) = \rho u_*^2(1+r_w)$
ϕ_z	Sediment exchange between the bottom and the water	$\phi_z = F_e - F_d$
Ψ	Porosity	-
Ω	Relaxation linearization of ζq_b	-

2. Splitting strategy for shallow water equations with non-constant density

For the sake of clearness, let us first apply the Lagrange-Projection (LP) strategy to system (1.1) without Exner equation or any source terms, namely

$$\begin{cases} \partial_t h + \partial_x(hu) = 0, \\ \partial_t(h\rho) + \partial_x(h\rho u) = 0, \\ \partial_t(h\rho u) + \partial_x(h\rho u^2 + p) = -gh\rho\partial_x z, \end{cases} \tag{2.1}$$

or alternatively in compact form

$$\partial_t \mathbf{Q} + \partial_x \mathbf{F}(\mathbf{Q}) = \mathbf{S}(\mathbf{Q}),$$

where $\mathbf{Q}$, $\mathbf{F}(\mathbf{Q})$ and $\mathbf{S}(\mathbf{Q})$ reduce themselves to

$$\mathbf{Q} = \begin{pmatrix} h \\ h\rho \\ h\rho u \end{pmatrix}, \quad \mathbf{F}(\mathbf{Q}) = \begin{pmatrix} hu \\ h\rho u \\ h\rho u^2 + p \end{pmatrix}, \quad \mathbf{S}(\mathbf{Q}) = \begin{pmatrix} 0 \\ 0 \\ -gh\rho\partial_x z \end{pmatrix}.$$

Afterwards, in Section 3, we will describe the general case, where the solid transport flux q_z is considered. Then, it is easy to prove that system (2.1) is hyperbolic. Indeed, its Jacobian matrix reads

$$\mathbf{J}(\mathbf{Q}) = \begin{pmatrix} u & -\dfrac{u}{\rho} & \dfrac{1}{\rho} \\ 0 & 0 & 1 \\ \dfrac{gh\rho}{2} & -u^2 + \dfrac{gh}{2} & 2u \end{pmatrix},$$

where the eigenvalues are given by $u, u \pm \bar{c}$ with $\bar{c} = \sqrt{gh}$ sound speed. Note that, in this particular case without solid transport flux, z is constant in time. Therefore, the quantity $gh\rho\partial_x z$ in the third equation is treated as a source term.

It is interesting to consider stationary solutions of this reduced model. Indeed, in practical applications, we find such steady states or perturbations of them. In the particular case of steady states with zero-velocity, we get the family

$$u = 0, \quad \partial_x(h+z) = -\frac{1}{2\rho}\partial_x(h\rho) + \frac{1}{2}\partial_x h, \tag{2.2}$$

or, written in alternative way,

$$u = 0, \quad \partial_x(h+z) = -\frac{h}{2\rho}\partial_x \rho. \tag{2.3}$$

Moreover, among all the stationary solutions (2.2), it is interesting to exhibit two particular families of steady states; the one with constant bed level

$$u = 0, \quad \frac{h^2\rho}{2} = \text{constant} \quad \text{and} \quad z = \text{constant}, \tag{2.4}$$

and the usual lake at rest solution

$$u = 0, \quad \rho = \text{constant} \quad \text{and} \quad H = h + z = \text{constant}. \tag{2.5}$$

When the friction and erosion-deposition source terms are neglected, we construct our numerical scheme in such a way that it exactly preserves the stationary solutions (2.4) and (2.5). That is, we want our numerical method to be exactly well-balanced for those stationary solutions (see for instance [2, 37]). Note that (2.4) and (2.5) are two particular families of the more general case (2.3). In Sections 2.2 and 4.1, we will see that the proposed schemes do not exactly preserve (2.3), but a discrete version of it. In such a case, we say that the numerical scheme is well-balanced with order 2 for (2.3), according to the definition introduced in [37]. Namely, the numerical scheme preserves a discrete stationary solution that is a second order approximation of (2.3).

2.1. Lagrange-projection decomposition

As mentioned in the introduction, the idea of the Lagrange-projection approach is to split the acoustic and transport terms of the model. In practice, this strategy can be explained by using Lagrangian coordinates. The approach then results in first considering the mathematical model formulated in Lagrangian coordinates and then perform the projection of the Lagrangian solution onto Eulerian coordinates. We shall detail both steps in what follows.

Let us first briefly recall the corresponding formalism. We consider a fluid particle located at position ξ at time $t = 0$ and then its trajectory through time or its characteristic curve $t \mapsto x(\xi, t)$

$$\begin{cases} \partial_t x(\xi,t) = u\big(x(\xi,t),t\big), \\ x(\xi,0) = \xi. \end{cases} \tag{2.6}$$

Then, any function $(x,t) \mapsto \varphi(x,t)$ in Eulerian coordinates can be expressed in Lagrangian coordinates as in the following:

$$(\xi,t) \mapsto \overline{\varphi}(\xi,t) = \varphi\big(x(\xi,t),t\big).$$

In particular, using the volume ratio $L(\xi,t)$,

$$L(\xi,t) = \partial_\xi x(\xi,t), \tag{2.7}$$

which satisfies

$$\begin{cases} \partial_t L(\xi,t) = \partial_\xi u\big(x(\xi,t),t\big), \\ L(\xi,0) = 1, \end{cases} \tag{2.8}$$

we can easily write the original system (2.1) in Lagrangian coordinates, namely

$$\begin{cases} \partial_t(L\bar{h}) = 0, \\ \partial_t(L\overline{h\rho}) = 0, \\ \partial_t(L\overline{h\rho u}) + \partial_\xi\left(g\bar{\rho}\dfrac{\bar{h}^2}{2}\right) = -g\bar{h}\bar{\rho}\partial_\xi\bar{z}. \end{cases} \tag{2.9}$$

More details about the Lagrange-projection decomposition applied to the shallow water system can be found for instance in [12, 48]. Let us remark that the Lagrangian formulation (2.9) will reveal itself to be very useful and convenient when trying to include the Exner equation in the model in Section 3. Indeed, we will see that it is easier to consider the Lagrangian formulation with the variable Lz rather than z, see [17].

Let us point out that system (2.9) may also be formulated in a different way. Indeed, observing that both $L\bar{h}$ and $L\bar{h}\bar{\rho}$ do not depend on time, we get

$$L\bar{h}(\xi,t) = L\bar{h}(\xi,0) = h(\xi,0) = h_0 \quad \text{and consequently} \quad L = \frac{h_0}{\bar{h}},$$

and therefore $0 = \partial_t(L\bar{h}\bar{\rho}) = L\bar{h}\partial_t\rho$, which means that

$$\partial_t\bar{\rho} = 0 \quad \text{and in particular} \quad \bar{\rho}(\xi,t) = \rho(\xi,0) = \rho_0.$$

Defining now the variables $\bar{\tau} = 1/\bar{h}$ and $\bar{\theta} = 1/\bar{\rho}$, we find the equivalent form of system (2.9),

$$\begin{cases} \partial_t\bar{\theta} = 0, \\ \partial_t(h_0\rho_0\bar{\tau}\bar{\theta}) - \partial_\xi\bar{u} = 0, \\ \partial_t(h_0\rho_0\bar{u}) + \partial_\xi\left(\dfrac{g}{2\bar{\tau}^2\bar{\theta}}\right) = -\dfrac{g}{\bar{\tau}\bar{\theta}}\partial_\xi\bar{z}, \end{cases}$$

and, alternatively, neglecting the bar for the sake of simplicity,

$$\begin{cases} \partial_t\theta = 0, \\ \partial_t(h_0\rho_0\tau\theta) - \partial_\xi u = 0, \\ \partial_t(h_0\rho_0 u) + \partial_\xi\left(\dfrac{g}{2\tau^2\theta}\right) = -\dfrac{g}{\tau\theta}\partial_\xi z. \end{cases} \tag{2.10}$$

In this framework, the numerical strategy could be once again summarized in two steps. First, we need to numerically solve the Lagrangian-acoustic system (2.9)-(2.10). Then, we project its solution into Eulerian coordinates. We will see that the most problematic part of this strategy will not be the approximation of the projection step but that of the Lagrangian system, especially when trying to satisfy the well-balanced property. In particular, for these equations (2.10), we describe an approximate Riemann solver which will be used to define the associated Godunov-type scheme. For this reason, it is convenient to reformulate system (2.10) exploiting the so-called mass variable m, which is given by $h_0\rho_0/\partial_\xi = \partial_m$. Thus, it is easy to show that Eqs. (2.10) are equivalent to the following system:

$$\begin{cases} \partial_t \theta = 0, \\ \partial_t(\tau\theta) - \partial_m u = 0, \\ \partial_t u + \partial_m p = -\dfrac{g}{\tau\theta}\partial_m z, \end{cases} \tag{2.11}$$

where we recall that $p = g\theta/(2(\tau\theta)^2)$. We will refer to Eqs. (2.11) as the acoustic system, as it can be obtained from the starting system (2.1) by considering only the acoustic phenomena and the topography variations. See [17, 22, 27] for more details about the acoustic-transport interpretation. Moreover, the eigenvalues of system (2.11) are given by 0 and $\pm h\rho\bar{c}$, where the latter are the speed of propagation of the acoustic waves; the material (transport) waves being related to the projection step. Thus, in situations in which the acoustic waves are much faster than the material ones, it can be very convenient to exploit an implicit approximation for the acoustic equations, obtaining in this way very fast implicit-explicit method. Further details about the implicit formulation for the acoustic system are given in Section 4.1. See also [19, 22, 26] for implicit-explicit Lagrange-projection numerical methods.

Looking for an approximate Riemann solver associated to system (2.11), we follow the Suliciu relaxation approach [55] and we introduce the following approximate relaxation system:

$$\begin{cases} \partial_t \theta = 0, \\ \partial_t(\tau\theta) - \partial_m u = 0, \\ \partial_t u + \partial_m \Pi = -\dfrac{g}{\tau\theta}\partial_m z, \\ \partial_t \Pi + a^2 \partial_m u = 0, \end{cases} \tag{2.12}$$

where Π is a new variable such that $\Pi = p$ at time $t = 0$. Our approximate Riemann solver will consist in an exact Riemann solver associated with system (2.12). Moreover, a^2 is a constant which linearizes $h^2\rho^2\bar{c}^2$ and which is taken as $a^2 \geq h^2\rho^2\bar{c}^2$ according to the sub-characteristic condition. Then, easy computations show that the eigenvalues of (2.12) are given by $\lambda = 0$, $\lambda_{\pm a} = \pm a$ and that the associated characteristic fields are all linearly degenerate. This property is well-known to provide an exact and easy solution of the Riemann problem. Indeed, we will obtain three waves that correspond to contact discontinuities. Then, exploiting the Rankine-Hugoniot relations across each wave, we are able to exactly define the solution of the Riemann problem associated to

system (2.12) (see for instance [33, 34] for more details). For applications related to the Suliciu relaxation approach, see for instance [5, 8, 19, 22, 23].

2.2. Approximate Riemann solver

In this section, we aim to briefly describe the approximate Riemann problem solution for system (2.11), which is found solving the Riemann problem associated with the relaxation system (2.12). The initial data of the Riemann problem are given by

$$(\theta, \tau\theta, u, \Pi)^T(m, t=0) = \begin{cases} (\theta_L, \tau_L\theta_L, u_L, \Pi_L)^T, & \text{if} \quad m < 0, \\ (\theta_R, \tau_R\theta_R, u_R, \Pi_R)^T, & \text{if} \quad m \geq 0, \end{cases}$$

where $\Pi_{L,R} = g(h^2\rho)_{L,R}/2$. Then, its solution would be composed of four different states separated by the three discontinuities,

$$\hat{\mathbf{U}}(m/t; \mathbf{U}_L, \mathbf{U}_R) = \begin{cases} \mathbf{U}_L, & \text{if} \quad m/t < \lambda_a^- = -a, \\ \mathbf{U}_L^*, & \text{if} \quad -a < m/t < \lambda_0 = 0, \\ \mathbf{U}_R^*, & \text{if} \quad 0 < m/t < \lambda_a^+ = a, \\ \mathbf{U}_R, & \text{if} \quad m/t > a, \end{cases}$$

where $\mathbf{U} = (\theta, \tau\theta, u, \Pi)^T$. The definition of $\mathbf{U}_L^*$ and $\mathbf{U}_R^*$ relies on the validity of the Rankine Hugoniot relations across each wave (recall that the characteristic fields are linearly degenerate) and, in particular, on a consistent approximation

$$\mathcal{M} = \mathcal{M}(\mathbf{U}_L, \mathbf{U}_R) = g\{h\rho\}_{ST}(z_R - z_L)$$

of the source term in (2.12), such that across the stationary wave one has

$$\begin{cases} u^* = u_L^* = u_R^*, \\ \Pi_R^* - \Pi_L^* + \mathcal{M} = 0. \end{cases} \tag{2.13}$$

Here, $\{h\rho\}_{ST}$ needs to be specified in a consistent way, namely

$$\lim_{\substack{h_L, h_R \to h \\ \rho_L, \rho_R \to \rho}} \{h\rho\}_{ST} = h\rho.$$

For the sake of brevity, we shall not give all the details here and we refer the reader to [22] for further informations. The star values $\mathbf{U}_L^*, \mathbf{U}_R^*$ are then given by

$$\theta_L^* = \theta_L, \tag{2.14a}$$

$$\theta_R^* = \theta_R, \tag{2.14b}$$

$$(\tau\theta)_L^* = \tau_L\theta_L + \frac{1}{a}(u^* - u_L), \tag{2.14c}$$

$$(\tau\theta)_R^* = \tau_R\theta_R - \frac{1}{a}(u^* - u_R), \tag{2.14d}$$

$$u^* = \frac{1}{2}(u_L + u_R) - \frac{1}{2a}(\Pi_R - \Pi_L) - \frac{\mathcal{M}}{2a}, \tag{2.14e}$$

$$\Pi_L^* = \frac{1}{2}(\Pi_L + \Pi_R) - \frac{a}{2}(u_R - u_L) + \frac{\mathcal{M}}{2}, \tag{2.14f}$$

$$\Pi_R^* = \frac{1}{2}(\Pi_L + \Pi_R) - \frac{a}{2}(u_R - u_L) - \frac{\mathcal{M}}{2}. \tag{2.14g}$$

2.2.1. Well-balanced property and definition of $\mathcal{M}$

The definition of $\mathcal{M}$ is driven by the well-balanced property. More precisely, assume that we want to preserve a discrete approximation of stationary solutions with zero-velocity, namely the ones defined in formula (2.2), and consider the following discretization of such stationary solutions:

$$(z_R - z_L) + \frac{h_R - h_L}{2} = -\frac{1}{2}\left\{\frac{1}{\rho}\right\}_{StS}(h_R\rho_R - h_L\rho_L), \tag{2.15}$$

where the term $\{1/\rho\}_{StS}$ needs to be specified and consistent such that

$$\lim_{\rho_L,\rho_R\to\rho}\left\{\frac{1}{\rho}\right\}_{StS} = \frac{1}{\rho}.$$

Hence, when $\mathbf{U}_L$ and $\mathbf{U}_R$ satisfy (2.15), we require $\mathbf{U}_L^* = \mathbf{U}_L$ and $\mathbf{U}_R^* = \mathbf{U}_R$ in order for the approximate Riemann solver to be well-balanced. On the one hand, (2.13) imposes

$$\Pi_R - \Pi_L + \mathcal{M} = 0, \quad \mathcal{M} = g\{h\rho\}_{ST}(z_R - z_L), \tag{2.16}$$

so that, inserting (2.15) into (2.16), we find

$$\begin{aligned}\frac{h_R^2\rho_R}{2} - \frac{h_L^2\rho_L}{2} &= -\{h\rho\}_{ST}(z_R - z_L)\\ &= \frac{1}{2}\{h\rho\}_{ST}\left(h_R - h_L + \left\{\frac{1}{\rho}\right\}_{StS}(h_R\rho_R - h_L\rho_L)\right).\end{aligned}$$

On the other hand, we have

$$\frac{h_R^2\rho_R}{2} - \frac{h_L^2\rho_L}{2} = \frac{1}{2}\left((h_R\rho_R - h_L\rho_L)\frac{h_R + h_L}{2} + (h_R - h_L)\left(\frac{h_R\rho_R + h_L\rho_L}{2}\right)\right).$$

Hence, a possibility is to set

$$\begin{cases}\{h\rho\}_{ST} = \dfrac{h_R\rho_R + h_L\rho_L}{2},\\ \left\{\dfrac{1}{\rho}\right\}_{StS} = \dfrac{1}{\{h\rho\}_{ST}}\dfrac{h_R + h_L}{2},\end{cases}$$

which is clearly consistent. In particular, we would define

$$\mathcal{M} = g\left(\frac{h_R\rho_R + h_L\rho_L}{2}\right)(z_R - z_L), \tag{2.17}$$

which allows us to preserve the stationary solutions which, according to (2.15), satisfy the following discretization:

$$(z_R - z_L) + \frac{h_R - h_L}{2} = -\frac{1}{2}\frac{h_R + h_L}{h_R\rho_R + h_L\rho_L}(h_R\rho_R - h_L\rho_L), \tag{2.18}$$

together with zero-velocity. Note that, if $\rho_L = \rho_R$ and $u_L = u_R = 0$, we recover the well-known lake at rest stationary solution (2.5) as (2.18) gives $h_L + z_L = h_R + z_R$. Moreover, the stationary solution (2.4) such that $z_L = z_R$, $u_L = u_R = 0$ and $\rho_L h_L^2 = \rho_R h_R^2$ gives $\mathcal{M} = 0$ and $u_L^* = u_L$, $u_R^* = u_R$ from (2.14). In other words, our scheme is well-balanced with order 2 for the stationary solutions (2.2) and it is exactly well-balanced for the stationary solutions (2.4) and (2.5).

Finally, observe that in practice the constant a is defined as in the following:

$$a = \max(\varepsilon, h_L\rho_L\bar{c}_L, h_R\rho_R\bar{c}_R),$$

where ε is a tolerance value so that a will not be zero. In practice, we take $\varepsilon = \Delta x$.

Remark 2.1. The proposed definition of $\mathcal{M}$ is not unique. Indeed, let us consider the following discretization of the stationary solutions based on (2.3) (instead of (2.2) above)

$$z_R + h_R - (z_L + h_L) = -\frac{1}{2}\left\{\frac{h}{\rho}\right\}_{StS}(\rho_R - \rho_L), \tag{2.19}$$

where the term $\{h/\rho\}_{StS}$ needs to be specified. Similar calculations lead to

$$\mathcal{M} = \frac{g}{2}\left(\frac{\rho_R + \rho_L}{2}\frac{h_R + h_L}{2} + \frac{h_R\rho_R + h_L\rho_L}{2}\right)(z_R - z_L), \tag{2.20}$$

which allows to preserve stationary solutions defined by (2.19) with

$$\left\{\frac{h}{\rho}\right\}_{StS} = \left(\frac{h_R + h_L}{2}\right)^2 \frac{8}{(\rho_R + \rho_L)(h_R + h_L) + 2(h_R\rho_R + h_L\rho_L)}.$$

Hence, in this section we have considered system (2.1) as a starting point to show how to include the evolution equation for the density variable in the Lagrange-projection approach. We have also defined an approximate Riemann solver for the resulting Lagrangian system. Let us now extend this strategy by including the Exner equation in the model.

3. Including the Exner equation in the splitting strategy

Moving to the following step, we now aim to include the Exner equation in the splitting strategy. Thus, we consider system (1.1) without source terms associated to friction and erosion-deposition processes, namely

$$\begin{cases} \partial_t h + \partial_x(hu) = 0, \\ \partial_t(h\rho) + \partial_x(h\rho u) = 0, \\ \partial_t(h\rho u) + \partial_x\left(h\rho u^2 + g\dfrac{h^2}{2}\rho\right) + gh\rho\partial_x z = 0, \\ \partial_t z + \zeta\partial_x q_z = 0. \end{cases} \tag{3.1}$$

In the following section, we show its Lagrangian-acoustic formulation with the aim of describing an associated approximate Riemann solver.

Referring to the previous works [17, 18], we consider two different strategies to take into account the Exner equation. In the first one, we update it directly in the projection step (Section 4.2), resembling an usual splitting strategy: we first approximate the shallow water equations with variable density and then also the topography is updated. Thus, here we do not have to give further details about its Lagrangian formulation. Moreover, we will see that this strategy could be particularly useful when considering the implicit-explicit version of the scheme. As for the second strategy, we propose to decouple the Exner equation in both steps, which would be the most natural approach in the Lagrange-projection framework, see next Section 3.1. Observe that even the latter strategy is only weakly-coupled and not fully-coupled in order to preserve the well-balanced property. Let us recall that decoupled approaches applied to the Exner system could produce unphysical oscillations in the numerical results due to the different eigenstructure of the shallow water model with and without the Exner equation (systems (2.1) and (3.1) respectively), see [24]. In this sense, the method that decouples the Exner equation in both steps proved to be more stable than the other one, especially at second-order of accuracy, refer to [17]. For this reason, here we consider and extend both strategies.

3.1. Updating the bed level in both steps

Exploiting once again the Lagrangian formalism introduced in Section 2.1, few computations allow us to write system (3.1) in Lagrangian coordinates, namely

$$\begin{cases} \partial_t(L\bar{h}) = 0, \\ \partial_t(L\overline{h\rho}) = 0, \\ \partial_t(L\overline{h\rho u}) + \partial_\xi\left(g\dfrac{\bar{h}^2}{2}\bar{\rho}\right) = -g\bar{h}\bar{\rho}\partial_\xi z, \\ \partial_t(L\overline{z}) - \partial_\xi(\overline{zu}) + \zeta\partial_\xi\overline{q_z} = 0, \end{cases} \tag{3.2}$$

or equivalently, using once again the change of variables $\bar{\tau} = 1/\bar{h}$ and $\bar{\theta} = 1/\bar{\rho}$,

$$\begin{cases} \partial_t\bar{\theta} = 0, \\ \partial_t(h_0\rho_0\bar{\tau}\bar{\theta}) - \partial_\xi\bar{u} = 0, \\ \partial_t(h_0\rho_0\bar{u}) + \partial_\xi\left(\dfrac{g}{2\bar{\tau}^2\bar{\theta}}\right) = -\dfrac{g}{\bar{\tau}\bar{\theta}}\partial_\xi\bar{z}, \\ \partial_t(h_0\rho_0\overline{z}) - \dfrac{\bar{u}}{\bar{\tau}\bar{\theta}}\partial_\xi\overline{z} + \dfrac{\zeta}{\bar{\tau}\bar{\theta}}\partial_\xi\overline{q_z} = 0. \end{cases} \tag{3.3}$$

Let us observe that the evolution equation for the bed elevation z is written as a conservation law in system (3.2), contrarily to the one in system (3.3). Then, neglecting the bars and exploiting again the mass variable m, the Lagrangian system (3.3) can also be reformulated as

$$\begin{cases} \partial_t \theta = 0, \\ \partial_t(\tau\theta) - \partial_m u = 0, \\ \partial_t u + \partial_m p = -\dfrac{g}{\tau\theta}\partial_m z, \\ \partial_t z - \dfrac{u}{\tau\theta}\partial_m z + \dfrac{\zeta}{\tau\theta}\partial_m q_z = 0. \end{cases}$$

Proceeding with the relaxation system, we consider the same variable Π to linearize the pressure term $p = gh^2\rho/2$, while for the solid transport discharge q_z we introduce Ω such that $\Omega = \zeta q_z$ at time $t = 0$ and suggest the linearized system

$$\begin{cases} \partial_t \theta = 0, \\ \partial_t(\tau\theta) - \partial_m u = 0, \\ \partial_t u + \partial_m \Pi = -\dfrac{g}{\tau\theta}\partial_m z, \\ \partial_t z - \dfrac{u}{\tau\theta}\partial_m z + \dfrac{1}{\tau\theta}\partial_m \Omega = 0, \\ \partial_t \Pi + a^2 \partial_m u = 0, \\ \partial_t \Omega + u^2\left(b^2\tau\theta - \dfrac{1}{\tau\theta}\right)\partial_m z + \dfrac{u}{\tau\theta}\partial_m \Omega = 0, \end{cases} \tag{3.4}$$

where the sub-characteristic condition is now given by $a^2 \geq h^2\rho^2\bar{c}^2$ and $u^2b^2 \geq (h\rho u)^2 + g(h\rho)^2\partial_u q_z$, $b > 0$, see [17]. In compact form, system (3.4) is equivalent to

$$\partial_t \mathbf{U} + \mathbf{A}(\mathbf{U})\partial_x \mathbf{U} = \mathbf{S}(\mathbf{U})$$

with

$$\mathbf{U} = \begin{pmatrix} \theta \\ \tau\theta \\ u \\ z \\ \Pi \\ \Omega \end{pmatrix}, \quad \mathbf{A}(\mathbf{U}) = \begin{pmatrix} 0 & 0 & 0 & 0 & 0 & 0 \\ 0 & 0 & -1 & 0 & 0 & 0 \\ 0 & 0 & 0 & 0 & 1 & 0 \\ 0 & 0 & 0 & -\dfrac{u}{\tau\theta} & 0 & \dfrac{1}{\tau\theta} \\ 0 & 0 & a^2 & 0 & 0 & 0 \\ 0 & 0 & 0 & u^2\left(b^2\tau\theta - \dfrac{1}{\tau\theta}\right) & 0 & \dfrac{u}{\tau\theta} \end{pmatrix},$$

$$\mathbf{S}(\mathbf{U}) = \begin{pmatrix} 0 \\ 0 \\ -\dfrac{g}{\tau\theta}\rho\partial_m z \\ 0 \\ 0 \\ 0 \end{pmatrix}. \tag{3.5}$$

Considering only the convective part of system (3.4), namely neglecting the term related to z in the third equation, we find that the eigenvalues are given by $\lambda = 0$, $\lambda_{\pm a} = \pm a$, $\lambda_{\pm b} = \pm|u|b$ and that once again the associated characteristic fields are all linearly degenerate. We remark that system (3.4) is not strictly hyperbolic anymore for $u = 0$ and that the eigenvalues are not ordered a priori, see again [17].

3.1.1. Approximate Riemann solver

Here we solve the Riemann problem associated to system (3.4) with initial data

$$(\theta, \tau\theta, u, z, \Pi, \Omega)^T(m, t = 0) = \begin{cases} (\theta_L, \tau_L\theta_L, u_L, z_L, \Pi_L, \Omega_L)^T, & \text{if} \quad m < 0, \\ (\theta_R, \tau_R\theta_R, u_R, z_R, \Pi_R, \Omega_R)^T, & \text{if} \quad m > 0 \end{cases}$$

with $\Pi_{L,R} = p_{L,R}$ and $\Omega_{L,R} = (\zeta q_z)_{L,R}$. Since the eigenvalues are not ordered a priori, at a continuous level there exists two different cases depending on whether $a < |u|b$ or not (recall that a and b are positive). In practice, we will distinguish between the following two cases $a < |u_L|b, a < |u_R|b$ and $a > |u^*|b$. As a consequence, if $a < |u_L|b, a < |u_R|b$, the solution reads

$$\hat{\mathbf{U}}(m/t; \mathbf{U}_L, \mathbf{U}_R) = \begin{cases} \mathbf{U}_L, & \text{if} \quad m/t < \lambda_b^- = -|u_L|b, \\ \mathbf{U}^*_{b,L}, & \text{if} \quad -|u_L|b < m/t < \lambda_a^- = -a, \\ \mathbf{U}^*_{a,L}, & \text{if} \quad -a < m/t < \lambda_0 = 0, \\ \mathbf{U}^*_{a,R}, & \text{if} \quad 0 < m/t < \lambda_a^+ = a, \\ \mathbf{U}^*_{b,R}, & \text{if} \quad a < m/t < \lambda_b^+ = |u_R|b, \\ \mathbf{U}_R, & \text{if} \quad m/t > |u_R|b \end{cases}$$

with

$$\mathbf{U}^*_{b,L} = \begin{pmatrix} \tau_L \\ u_L \\ z^* \\ \Pi_L \\ \Omega^* \end{pmatrix}, \quad \mathbf{U}^*_{a,L} = \begin{pmatrix} \tau_L^* \\ u^* \\ z^* \\ \Pi_L^* \\ \Omega^* \end{pmatrix}, \quad \mathbf{U}^*_{a,R} = \begin{pmatrix} \tau_R^* \\ u^* \\ z^* \\ \Pi_R^* \\ \Omega^* \end{pmatrix}, \quad \mathbf{U}^*_{b,R} = \begin{pmatrix} \tau_R \\ u_R \\ z^* \\ \Pi_R \\ \Omega^* \end{pmatrix}. \tag{3.6}$$

On the other hand, if $a > |u^*|b$, the solution is given by

$$\hat{\mathbf{U}}(m/t; \mathbf{U}_L, \mathbf{U}_R) = \begin{cases} \mathbf{U}_L, & \text{if} \quad m/t < -a, \\ \mathbf{U}^*_{a,L}, & \text{if} \quad -a < m/t < -|u^*|b, \\ \mathbf{U}^*_{b,L}, & \text{if} \quad -|u^*|b < m/t < 0, \\ \mathbf{U}^*_{b,R}, & \text{if} \quad 0 < m/t < |u^*|b, \\ \mathbf{U}^*_{a,R}, & \text{if} \quad |u^*|b < m/t < a, \\ \mathbf{U}_R, & \text{if} \quad m/t > a \end{cases}$$

with

$$\mathbf{U}^*_{a,L} = \begin{pmatrix} \tau^*_L \\ u^* \\ z_L \\ \Pi^*_L \\ \Omega_L \end{pmatrix}, \quad \mathbf{U}^*_{b,L} = \begin{pmatrix} \tau^*_L \\ u^* \\ z^* \\ \Pi^*_L \\ \Omega^* \end{pmatrix}, \quad \mathbf{U}^*_{b,R} = \begin{pmatrix} \tau^*_R \\ u^* \\ z^* \\ \Pi^*_R \\ \Omega^* \end{pmatrix}, \quad \mathbf{U}^*_{a,R} = \begin{pmatrix} \tau^*_R \\ u^* \\ z_R \\ \Pi^*_R \\ \Omega_R \end{pmatrix}. \tag{3.7}$$

In order to define the star states in (3.6) and (3.7), we exactly follow the same lines as in Section 2.2. In particular, it is worth noticing that z and Ω are constant through the waves with $\pm a$-velocity and zero-velocity, therefore we only need to find a single star value z^*, Ω^* for these two variables. Similarly for the variables θ, τ, u and Π, since they are constant through the waves with $\pm|u|b$-velocity, at most two star values are necessary. This property is related to the fact that in the third equation we treat the coupling term $-g\partial_m z/\tau\theta$ as a source term.

Moreover, in both cases we exploit the same star values for the variables $\theta, \tau\theta, u$, given by (2.14) and (2.17). Regarding z^* and Ω^*, we need to separate the two cases and, in particular, if $a < |u_L|b$ and $a < |u_R|b$, we get

$$\begin{cases} z^* = \dfrac{|u_R|\big(\operatorname{sign}(u_R) + b\tau_R\theta_R\big)z_R - |u_L|\big(\operatorname{sign}(u_L) - b\tau_L\theta_L\big)z_L}{|u_R|(\operatorname{sign}(u_R) + b\tau_R\theta_R) - |u_L|(\operatorname{sign}(u_L) - b\tau_L\theta_L)} \\ \qquad - \dfrac{\Omega_R - \Omega_L}{|u_R|(\operatorname{sign}(u_R) + b\tau_R\theta_R) - |u_L|(\operatorname{sign}(u_L) - b\tau_L\theta_L)}, \\ \Omega^* = \dfrac{\Omega_R + \Omega_L}{2} + \dfrac{|u_R|}{2}(\operatorname{sign}(u_R) + b\tau_R\theta_R)(z^* - z_R) \\ \qquad + \dfrac{|u_L|}{2}(\operatorname{sign}(u_L) - b\tau_L\theta_L)(z^* - z_L), \end{cases} \tag{3.8}$$

otherwise we state

$$\begin{cases} (z|u|)^* = |u^*|\dfrac{\big(\operatorname{sign}(u^*) + b\tau^*_R\theta_R\big)z_R - \big(\operatorname{sign}(u^*) - b\tau^*_L\theta_L\big)z_L}{b\big(\tau^*_R\theta_R + \tau^*_L\theta_L\big)} \\ \qquad - \dfrac{\Omega_R - \Omega_L}{b\big(\tau^*_R\theta_R + \tau^*_L\theta_L\big)}, \\ \Omega^* = \dfrac{\Omega_R + \Omega_L}{2} + \dfrac{1}{2}\big((\operatorname{sign}(u^*) + b\tau^*_R\theta_R)\big((z|u|)^* - |u^*|z_R\big) \\ \qquad\qquad + (\operatorname{sign}(u^*) - b\tau^*_L\theta_L)((z|u|)^* - |u^*|z_L)\big). \end{cases} \tag{3.9}$$

Finally, the parameters a and b are defined as $a = \max(\Delta x, h_L\rho_L\bar{c}_L, h_R\rho_R\bar{c}_R)$ and

$$b = \max\left(\varepsilon, \sqrt{(h_L\rho_L)^2 + g\frac{(h_L\rho_L)^2}{u_L^2}\partial_u(q_b)_L}, \sqrt{(h_R\rho_R)^2 + g\frac{(h_R\rho_R)^2}{u_R^2}\partial_u(q_b)_R}\right). \tag{3.10}$$

However, since assuming $a \geq |u_L|b$ or $a \geq |u_R|b$ does not necessarily imply that $a > |u^*|b$, in practice we need to do the following. If a and b are such that $a \geq |u_L|b$

or $a \geq |u_R|b$ but $a \leq |u^*|b$, we need to increase the value of a and redefine it as $a = (1+\epsilon)|u^*|b$ (with typically $\epsilon = 0.01$). We underline that, once we have redefined a, we have to recompute the value of u^*, and more generally the quantities in (2.14). In practice, this iterative process usually converges in one or two iterations. See again the previous work [17] for more details about this approximate Riemann solver applied to system (3.2) with constant density ρ in time and space.

Finally, let us remark that the choice not to use a fully coupled approximation for this system also contributes to the fulfillment of the well-balanced property, namely to the preservation of the stationary solutions (2.2). Indeed, uz^* and Ω^* are automatically equal to zero when the steady state condition (2.2) is satisfied.

4. Numerical method

Notation. First, we define the constant space step Δx and constant time step Δt. The mesh interfaces are given by $x_{j+1/2} = j\Delta x$ for $j \in \mathbb{Z}$ and the intermediate times by $t^n = n\Delta t$ for $n \in \mathbb{N}$. At each time t^n, we seek for an approximation $\mathbf{Q}_j^n$ of the solution in the interval $[x_{j-1/2}, x_{j+1/2})$, $j \in \mathbb{Z}$. Therefore, a piecewise constant approximate solution $x \to \mathbf{Q}_{\Delta t,\Delta x}(x,t^n)$ of the solution $\mathbf{Q}$ is given by

$$\mathbf{Q}_{\Delta t,\Delta x}(x,t^n) = \mathbf{Q}_j^n \quad \text{for all} \quad x \in C_j = [x_{j-1/2}; x_{j+1/2}), \quad j \in \mathbb{Z}, \quad n \in \mathbb{N}.$$

Numerical strategy. As it has already been explained in the previous sections, the numerical scheme consists of three steps: first one has to solve the acoustic-Lagrangian step, then the transport-projection one and, finally, we need to include the source terms. Thus, using the above notations and Lagrangian coordinates we have

1. Update $\mathbf{Q}^n$ to $L\mathbf{Q}^{n+}$ solving the Lagrangian system (Section 4.1).
2. Project $L\mathbf{Q}^{n+}$ into Eulerian coordinates, finding $\mathbf{Q}^{n+1-}$ (Section 4.2).
3. Consider the erosion, deposition and friction source terms and update $\mathbf{Q}^{n+1-}$ to $\mathbf{Q}^{n+1}$ (Section 4.3).

4.1. Lagrangian step

As we have already anticipated, in order to approximate the acoustic or Lagrangian step, we exploit a first-order Godunov-type scheme associated with the approximate Riemann solver for the acoustic system that we have built in the previous sections. Since the approximate Riemann problem solution appears to be the same for the variables τ, θ and u both with and without the contribution of the Exner equation, we can immediately write their numerical approximation. Indeed, we have

$$\begin{cases} L_j^{n+} h_j^{n+} = L_j^n h_j^n, \\ L_j^{n+} h_j^{n+} \rho_j^{n+} = L_j^n h_j^n \rho_j^n, \\ L_j^{n+} (h\rho u)_j^{n+} = L_j^n (h\rho u)_j^n - \dfrac{\Delta t}{\Delta x}\big(\Pi^*_{j+1/2} - \Pi^*_{j-1/2}\big) - \Delta t\{gh\rho\partial_x z\}_j^n, \end{cases} \tag{4.1}$$

where

$$L_j^{n+} = L_j^n + \frac{\Delta t}{\Delta x}\big(u^*_{j+1/2} - u^*_{j-1/2}\big), \quad L_j^n = 1 \tag{4.2}$$

with star values $u^*_{j+1/2}, \Pi^*_{j+1/2}$ being locally defined at each interface $x_{j+1/2}$ using formulas (2.14). For the source term, we simply state

$$s_j^n = \{gh\rho\partial_x z\}_j^n = \frac{1}{2}\big(s^n_{j+1/2} + s^n_{j-1/2}\big), \quad s^n_{j+1/2} = -\frac{\mathcal{M}^n_{j+1/2}}{\Delta x}, \tag{4.3}$$

and

$$\mathcal{M}^n_{j+1/2} = \mathcal{M}\left((h_j^n, h_j^n\rho_j^n; z_j^n); (h_{j+1}^n, h_{j+1}^n\rho_{j+1}^n; z_{j+1}^n)\right), \quad \forall j$$

given by (2.20). Few algebraic computations give a completely equivalent numerical approximation for the relaxation acoustic system (2.12), namely

$$\begin{cases} \theta_j^{n+} = \theta_j^n, & \text{(4.4a)} \\ \tau\theta_j^{n+} = \tau\theta_j^n + \dfrac{\Delta t}{\Delta m_j}\big(u^*_{j+1/2} - u^*_{j-1/2}\big), & \text{(4.4b)} \\ u_j^{n+} = u_j^n - \dfrac{\Delta t}{\Delta m_j}\big(\Pi^*_{j+1/2} - \Pi^*_{j-1/2}\big) - \Delta t\left\{\dfrac{g}{\tau\theta}\partial_m z\right\}_j^n, & \text{(4.4c)} \\ \Pi_j^{n+} = \Pi_j^n - \big(a^n_{j+1/2}\big)^2\dfrac{\Delta t}{\Delta m_j}\big(u^*_{j+1/2} - u^*_{j-1/2}\big). & \text{(4.4d)} \end{cases}$$

Remark 4.1. It is particularly useful to show the latter formulation as it can be interpreted in an implicit way by defining the star values as in the following:

$$\begin{aligned} u^*_{j+1/2} &= \frac{1}{2}\big(u^{n+}_{j+1} + u^{n+}_j\big) - \frac{1}{2a^n_{j+1/2}}\big(\Pi^{n+}_{j+1} - \Pi^{n+}_j\big) - \frac{\mathcal{M}^n_{j+1/2}}{2a^n_{j+1/2}}, \\ \Pi^*_{j+1/2} &= \frac{1}{2}\big(\Pi^{n+}_{j+1} + \Pi^{n+}_j\big) - \frac{a^n_{j+1/2}}{2}\big(u^{n+}_{j+1} - u^{n+}_j\big). \end{aligned} \tag{4.5}$$

Hence, for an implicit approximation of the acoustic step, we highlight that first we solve the evolution equations for u and Π and then we use the obtained solution to compute $\tau\theta^{n+}$. In particular, the Eqs. (4.4c) and (4.4d) can be reformulated as a linear system and, as such, their resolution is not computationally expensive. Here we do not provide further details, see either Appendix A or refer respectively to [19, 22] for this approach applied to the shallow water equations and to the gas dynamics equations.

Then, let us focus on the numerical approximation of the topography by considering the two different possibilities already described.

Exner equation in the projection step. It is evident that in this case we simply have $z^{n+} = z^n$ as the Exner equation is completely taken into account in the transport system. As such, for the stability of the numerical scheme, we ask for the following CFL condition for the time step:

$$\Delta t \leq \mathrm{CFL}_l \frac{\Delta x}{\max_j\{\max(\tau_j^n\theta_j^n, \tau_{j+1}^n\theta_{j+1}^n)\max(a_{j+1/2})\}} \tag{4.6}$$

with CFL_l a constant value. Clearly, we do not need anymore condition (4.6) if we use the implicit version of the numerical approximation.

Exner equation in both steps. Using the approximate Riemann solver presented in Section 3.1.1, here we state

$$L_j^{n+}z_j^{n+} = L_j^n z_j^n - \frac{\Delta t}{\Delta x}\big((\Omega - zu)^*_{j+1/2} - (\Omega - zu)^*_{j-1/2}\big). \tag{4.7}$$

Let us remark that we could envisage to compute implicitly the variables Lz and $L\Omega$ as well without an excessive computational cost. Indeed, once we have found u^{n+}, Π^{n+} and τ^{n+} by solving the implicit linear system given by formula (4.5), the star values $z^{*,n+}$ and $\Omega^{*,n+}$ lead to another linear system thanks to the fact that u^{n+}, Π^{n+} and τ^{n+} are now fixed values.

In this case, the CFL condition on the time step for the explicit approximation is given by

$$\Delta t \leq \mathrm{CFL}_l \frac{\Delta x}{\max_j\big\{\max(\tau_j^n\theta_j^n, \tau_{j+1}^n\theta_{j+1}^n)\max(a_{j+1/2}, (|u|b)_{j+1/2})\big\}}. \tag{4.8}$$

4.2. Projection step

In this section we present the numerical approximation for the projection step. Since it has already been presented in different papers for other systems, here we give few details about it (see for instance [17, 27, 48]).

Aiming to project the Lagrangian solution into Eulerian coordinates, we consider the following identity:

$$\int_{\xi_1}^{\xi_2} L(\xi,t)X(\xi,t)d\xi = \int_{x(\xi_1,t)}^{x(\xi_2,t)} X(x,t)dx$$

with $X = h, h\rho, h\rho u$ and, if needed, $X = z$. Then, we define $\hat{\xi}_{j+1/2}$ such that

$$x\big(\hat{\xi}_{j+1/2}, t^{n+1}\big) = x_{j+1/2}, \quad x\big(\hat{\xi}_{j+1/2}, t^n\big) = \hat{\xi}_{j+1/2} \quad \text{for all} \quad j.$$

Subsequently, we can start writing

$$\begin{aligned} X_j^{n+1} &= \frac{1}{\Delta x}\int_{x_{j-1/2}}^{x_{j+1/2}} X(x,t^{n+1})dx \\ &= \frac{1}{\Delta x}\int_{x(\hat{\xi}_{j-1/2},t^{n+1})}^{x(\hat{\xi}_{j+1/2},t^{n+1})} X(x,t^{n+1})dx \\ &= \frac{1}{\Delta x}\int_{\hat{\xi}_{j-1/2}}^{\hat{\xi}_{j+1/2}} L(\xi,t^{n+1-})X(\xi,t^{n+1-})d\xi, \end{aligned}$$

and splitting the last integral into three parts

$$\begin{aligned}
&\frac{1}{\Delta x}\int_{\hat{\xi}_{j-1/2}}^{\hat{\xi}_{j+1/2}} L(\xi,t^{n+1-})X(\xi,t^{n+1-})d\xi \\
&= \frac{1}{\Delta x}\int_{\hat{\xi}_{j-1/2}}^{\xi_{j-1/2}} L(\xi,t^{n+1-})X(\xi,t^{n+1-})d\xi \\
&\quad + \frac{1}{\Delta x}\int_{\xi_{j-1/2}}^{\xi_{j+1/2}} L(\xi,t^{n+1-})X(\xi,t^{n+1-})d\xi \\
&\quad + \frac{1}{\Delta x}\int_{\xi_{j+1/2}}^{\hat{\xi}_{j+1/2}} L(\xi,t^{n+1-})X(\xi,t^{n+1-})d\xi. \qquad (4.9)
\end{aligned}$$

Then, estimating $\hat{\xi}_{j+1/2}$ such that

$$x_{j+1/2} = x\big(\hat{\xi}_{j+1/2},t^{n+1}\big) \simeq x\big(\hat{\xi}_{j+1/2},t^{n}\big) + \Delta t\partial_t x\big(\hat{\xi}_{j+1/2},t^{n}\big) \simeq \hat{\xi}_{j+1/2} + \Delta t u^*_{j+1/2},$$

we approximate the last three integrals in (4.9) and obtain

$$X_j^{n+1-} = (LX)_j^{n+} - \frac{\Delta t}{\Delta x}\big(u^*_{j+1/2}(LX)^{n+}_{j+1/2} - u^*_{j-1/2}(LX)^{n+}_{j-1/2}\big), \qquad (4.10)$$

where for all j

$$(LX)^{n+}_{j+1/2} = \begin{cases} (LX)^{n+}_j, & \text{if} \quad u^*_{j+1/2} \geq 0, \\ (LX)^{n+}_{j+1}, & \text{if} \quad u^*_{j+1/2} < 0. \end{cases}$$

For the projection step, the CFL condition on the time step is the following:

$$\Delta t \leq \mathrm{CFL}_t \frac{\Delta x}{\max_j\big\{u^+_{j-1/2} - u^-_{j+1/2}\big\}} \qquad (4.11)$$

with CFL_t a constant value and

$$u^+_{j-1/2} = \max\big(u^*_{j-1/2},0\big), \quad u^-_{j+1/2} = \min\big(u^*_{j+1/2},0\big).$$

As for the final time step, we take the minimum between the Lagrangian and projection ones. Then, we only need to specify the numerical approximation of the topography.

Exner equation in the transport step. Referring to the previous work [18], for the numerical approximation of the Exner equation we state

$$z_j^{n+1-} = z_j^n - \zeta\frac{\Delta t}{\Delta x}\left(u^*_{j+1/2}\left(\frac{q_b}{u}\right)^{n+}_{j+1/2} - u^*_{j-1/2}\left(\frac{q_b}{u}\right)^{n+}_{j-1/2}\right), \qquad (4.12)$$

where

$$\left(\frac{q_b}{u}\right)^{n+}_{j+1/2} = \begin{cases} \left(\frac{q_b}{u}\right)\left((L\mathbf{Q})^{n+}_{j+1}\right), & \text{if} \quad u^*_{j+1/2} \leq 0, \\ \left(\frac{q_b}{u}\right)\left((L\mathbf{Q})^{n+}_{j}\right), & \text{if} \quad u^*_{j+1/2} > 0. \end{cases}$$

Exner equation in both steps. In this case the numerical approximation for z is similar to the one of the other variables with the only difference that, in the numerical flux, we use the values z_j^{n+} instead of its Lagrangian counterpart $(Lz)_j^{n+}$. Namely, we state

$$z_j^{n+1-} = (Lz)_j^{n+} - \frac{\Delta t}{\Delta x}\big(u^*_{j+1/2} z^{n+}_{j+1/2} - u^*_{j-1/2} z^{n+}_{j-1/2}\big). \tag{4.13}$$

This choice is actually related to the second-order extension of this scheme, for which we refer to [17].

For the reader's sake, let us summarize which formulas we use for each scheme:

- Explicit scheme with topography only updated at the end of the transport step: formulas (4.4), (4.10), (4.12).
- Implicit-explicit scheme with topography only updated at the end of the transport step: formulas (4.4), (4.5), (4.10), (4.12).
- Explicit scheme with topography updated in both the acoustic and transport step: formulas (4.4), (4.7), (4.10), (4.13).

Finally, let us sum up the properties of the numerical schemes we presented so far in the following theorem.

Theorem 4.1. *Consider the three LP numerical schemes we presented so far, namely the explicit method with Exner equation in the transport step (formulas* (4.4)*,* (4.10)*,* (4.12)*), its implicit-explicit version (formulas* (4.4)*,* (4.5)*,* (4.10)*,* (4.12)*) and finally the scheme with Exner equation in both steps (formulas* (4.4)*,* (4.7)*,* (4.10)*,* (4.13)*).*

a) The above-mentioned numerical schemes are well-balanced in the following sense. They are able to exactly preserve the stationary solutions (2.4)-(2.5)*. Whereas, concerning the steady state* (2.2)*, the methods are well-balanced with order two: they preserve its second-order discretization* (2.15)*.*

b) Under the CFL condition (4.11) *with* $\mathrm{CFL}_t = 0.5$*, the above-mentioned numerical schemes preserve the positivity of the water height* h*.*

c) Under the CFL condition (4.11) *with* $\mathrm{CFL}_t = 0.5$*, the assumption of the positivity of the water height (point b) and of* $h_j^{n+1-} \neq 0 \ \forall j$*, if* $\rho_w \leq \rho_j^n \leq \rho_s \ \forall j$*, then it follows that* $\rho_w \leq \rho_j^{n+1-} \leq \rho_s \ \forall j$*. This statement is true for any of the above-mentioned numerical schemes.*

Proof.

a) The well-balanced property results from the definition of the approximate Riemann solver presented in Section 2.2 (Section 3.1.1 with the Exner equation). In particular, in the acoustic step we find $u^*_{j+1/2} = 0 \ \forall j$ and $L\mathbf{Q}_j^{n+} = \mathbf{Q}_j^n$ after few computations. Then, regarding the transport step, it is enough to observe that $\mathbf{Q}_j^{n+1-} = L\mathbf{Q}_j^{n+}$ as $u^*_{j+1/2} = 0$. Finally, observe that at this stage the source terms

are not considered, otherwise the stationary solutions would no longer be such. For this reason, we automatically have $\mathbf{Q}_j^{n+1} = \mathbf{Q}_j^{n+1-}$.

b) Assume $h_j^n \geq 0 \ \forall j$. It is straightforward to see that $L_j^{n+} h_j^{n+} \geq 0 \ \forall j$ from discretization (4.1). Furthermore, given $h_j^n > 0$ we can also show that $h_j^{n+} > 0$ under the CFL condition (4.11) with $\mathrm{CFL}_t = 1$.

Then, considering the transport approximation (4.10) with $X = h$, we have

$$\begin{aligned} h_j^{n+1-} &= L_j^{n+} h_j^{n+} - \frac{\Delta t}{\Delta x}\left(u^*_{j+1/2}(Lh)^{n+}_{j+1/2} - u^*_{j-1/2}(Lh)^{n+}_{j-1/2}\right) \\ &= L_j^{n+} h_j^{n+} - \frac{\Delta t}{\Delta x}\Big((u^*_{j+1/2})^+(Lh)^{n+}_j + (u^*_{j+1/2})^-(Lh)^{n+}_{j+1} \\ &\qquad\qquad - (u^*_{j-1/2})^+(Lh)^{n+}_{j-1} - (u^*_{j-1/2})^-(Lh)^{n+}_j\Big) \\ &= L_j^{n+} h_j^{n+}\left(1 - \frac{\Delta t}{\Delta x}\left((u^*_{j+1/2})^+ - (u^*_{j-1/2})^-\right)\right) \\ &\quad - \frac{\Delta t}{\Delta x}\left((u^*_{j+1/2})^-(Lh)^{n+}_{j+1} - (u^*_{j-1/2})^+(Lh)^{n+}_{j-1}\right). \end{aligned}$$

Then, it is clear that

$$-\frac{\Delta t}{\Delta x}\left((u^*_{j+1/2})^-(Lh)^{n+}_{j+1} - (u^*_{j-1/2})^+(Lh)^{n+}_{j-1}\right) \geq 0.$$

Hence, if

$$\frac{\Delta t}{\Delta x}\left((u^*_{j+1/2})^+ - (u^*_{j-1/2})^-\right) \leq 1, \tag{4.14}$$

we have $h_j^{n+1-} \geq 0$. Finally, let us observe that condition (4.11) with $\mathrm{CFL}_t = 0.5$ implies condition (4.14).

c) Let us assume that $\rho_w \leq \rho_j^n \leq \rho_s \ \forall j$. To prove that $\rho_w \leq \rho_j^{n+1-} \leq \rho_s \ \forall j$, we start by showing that $\rho_w \leq \rho_j^{n+1-} \ \forall j$ and then that $\rho_j^{n+1-} \leq \rho_s \ \forall j$. We also assume $h_j^n \geq 0$ and $h_j^{n+1-} > 0$.

First of all, we define the new variable $\tilde{\rho} = \rho - \rho_w$. As such, it is clear that its evolution equation is given by $\partial_t(h\tilde{\rho}) + \partial_x(h\tilde{\rho}u) = 0$ and its approximation reads

$$\begin{aligned} (h\tilde{\rho})_j^{n+1-} &= (Lh\tilde{\rho})_j^{n+} - \frac{\Delta t}{\Delta x}\left(u^*_{j+1/2}(Lh\rho)^{n+}_{j+1/2} - u^*_{j-1/2}(Lh\rho)^{n+}_{j-1/2}\right) \\ &\quad + \rho_w \frac{\Delta t}{\Delta x}\left(u^*_{j+1/2}(Lh)^{n+}_{j+1/2} - u^*_{j-1/2}(Lh)^{n+}_{j-1/2}\right) \\ &= (Lh\tilde{\rho})_j^{n+} - \frac{\Delta t}{\Delta x}\left(u^*_{j+1/2}(Lh\tilde{\rho})^{n+}_{j+1/2} - u^*_{j-1/2}(Lh\tilde{\rho})^{n+}_{j-1/2}\right). \end{aligned}$$

Now, we aim to prove that $\tilde{\rho}_j^{n+1-} \geq 0$, namely that $\rho_j^{n+1-} \geq \rho_w$. Hence, we use the same strategy as in point (b). We have

$$\begin{aligned}
(h\tilde{\rho})_j^{n+1-} &= (Lh\tilde{\rho})_j^{n+} - \frac{\Delta t}{\Delta x}\left(u^*_{j+1/2}(Lh\tilde{\rho})^{n+}_{j+1/2} - u^*_{j-1/2}(Lh\tilde{\rho})^{n+}_{j-1/2}\right) \\
&= (Lh\tilde{\rho})_j^{n+} - \frac{\Delta t}{\Delta x}\Big((u^*_{j+1/2})^+(Lh\tilde{\rho})_j^{n+} + (u^*_{j+1/2})^-(Lh\tilde{\rho})_{j+1}^{n+} \\
&\qquad\qquad - (u^*_{j-1/2})^+(Lh\tilde{\rho})_{j-1}^{n+} - (u^*_{j-1/2})^-(Lh)_j^{n+}\Big) \\
&= (Lh\tilde{\rho})_j^{n+}\left(1 - \frac{\Delta t}{\Delta x}\left((u^*_{j+1/2})^+ - (u^*_{j-1/2})^-\right)\right) \\
&\quad - \frac{\Delta t}{\Delta x}\left((u^*_{j+1/2})^-(Lh\tilde{\rho})_{j+1}^{n+} - (u^*_{j-1/2})^+(Lh\tilde{\rho})_{j-1}^{n+}\right),
\end{aligned}$$

and then, as in point (b), it follows that $(h\tilde{\rho})_j^{n+1-} \geq 0$ under condition (4.11) with $\mathrm{CFL}_t = 0.5$. Namely, we found $\rho_j^{n+1-} \geq \rho_w$ as we already know that $h_j^{n+1-} > 0$.

As a second step, we want to prove that $\rho_j^{n+1-} \leq \rho_s$. This time we define the variable $\tilde{\rho} = \rho_s - \rho$, whose approximation reads

$$(h\tilde{\rho})_j^{n+1-} = (Lh\tilde{\rho})_j^{n+} - \frac{\Delta t}{\Delta x}\left(u^*_{j+1/2}(Lh\tilde{\rho})^{n+}_{j+1/2} - u^*_{j-1/2}(Lh\tilde{\rho})^{n+}_{j-1/2}\right)$$

once again. Then, we just follow the same strategy as before to prove that $\tilde{\rho}_j^{n+1-} \geq 0$ and thus $\rho_s \geq \rho_j^{n+1-}$. □

4.3. Including the source terms for friction and erosion/deposition fluxes

The last step consists in including the erosion, deposition and friction terms in the mathematical model. Following the lines of [39], we aim at exploiting a semi-implicit approximation for the source terms. Hence, considering first the variables $h\rho$ and z, their updating formulas read

$$\begin{cases}
h_j^{n+1}\rho_j^{n+1} = h_j^{n+1-}\rho_j^{n+1-} \\
\qquad\qquad + \Delta t\zeta\rho_z\left((1-\Psi)v_s E_{s,j}^{n+1-}\frac{z_j^{n+1}}{z_j^{n+1-}} - v_s c_{z,j}^{n+1-}\frac{h_j^{n+1}\rho_j^{n+1}}{h_j^{n+1-}\rho_j^{n+1-}}\right), \\
z_j^{n+1} = z_j^{n+1-} - \Delta t\zeta\left((1-\Psi)v_s E_{s,j}^{n+1-}\frac{z_j^{n+1}}{z_j^{n+1-}} - v_s c_{z,j}^{n+1-}\frac{h_j^{n+1}\rho_j^{n+1}}{h_j^{n+1-}\rho_j^{n+1-}}\right),
\end{cases} \tag{4.15}$$

where we recall that

$$\phi_z = F_e - F_d, \quad F_e = (1-\Psi)v_s E_s, \quad F_d = v_s c_z.$$

Then, the solution of this linear system (4.15) can be explicitly found, we just refer to [39] for more details about it. Subsequently, as we have found $h_j^{n+1}\rho_j^{n+1}$ and z_j^{n+1}, we can automatically define ϕ_z as

$$\phi_z = \frac{1-\Psi}{\rho_z\Delta t}\left(h_j^{n+1}\rho_j^{n+1} - h_j^{n+1-}\rho_j^{n+1-}\right),$$

and thus update h_j^{n+1} and $(h\rho u)_j^{n+1}$, for which the friction term is treated semi-implicitly as well, see [39] for more details.

Remark 4.2. The numerical treatment for the erosion and deposition terms correspond to the approach used in [39]. Following the same ideas, one can prove that, provided that both $h\rho_j^{n+1-}$ and z_j^{n+1-} are positive, $h\rho_j^{n+1}$ and z_j^{n+1} remain positive. Let us remark that the positivity of z is not a requirement in the case of the model presented here, where the sediment bed is assumed to be as large as required and erosion is limited. Nevertheless this is not usually the case in practical situations where we have a limited erodible bed. In such scenarios this condition would be relevant, which justifies this approach. The result easily follows only for $h\rho_j^{n+1}$ if no limitation for the erodible bottom is made.

5. Numerical simulations

This section is devoted to the presentation of the numerical results. Here we consider the three different numerical methods we have presented so far. For the sake of brevity, we call them as in the following:

- LP-TrZ if the topography is updated at the end of the transport step and the approximation of the acoustic step is explicit;
- LP-TrZ-Imp if the topography is updated at the end of the transport step and the approximation of the acoustic step is implicit;
- LP-AcTrZ if the topography is updated in both the acoustic and transport step.

If not otherwise specified, in the numerical simulations we take $\mathrm{CFL}_l = 0.45$ and $\mathrm{CFL}_t = 0.99$. Finally, we underline that for all the numerical simulations, we exploited MATLAB language with a single Intel Core i7 CPU.

5.1. Lake at rest solution with suspended sediment

In [39], it has been presented the following numerical test, which is useful to check if our numerical scheme produces indeed the physical solution described in Section 1. We consider a closed channel of length $L = 2$ m, where the water is still $u = 0$, the free surface is constant in space ($h + z = 3$ m) as well as the bed height ($z = 1.05$ m). Then, the diameter of the sediments is given by $d = 3.9$ mm and the sediment concentration is $c(x, t) = 0.2$. Finally, we also impose the following parameter values, $\rho_s = 1.580$, $\theta_c^* = 0.045$ and $\mu_f = 0.03$. The solution is computed at final time $t_{End} = 30$ s. As explained in Section 1, we expect the bed level to increase due to sediment deposition and, consequently, the water height to decrease as the free surface should remain constant in time. Moreover, the velocity should remain null as the channel is closed and the pressure term is constant in the domain. Finally, since $c < 1 - \Psi$, the density of the mixture water sediment is expected to decrease. All these remarks are indeed verified

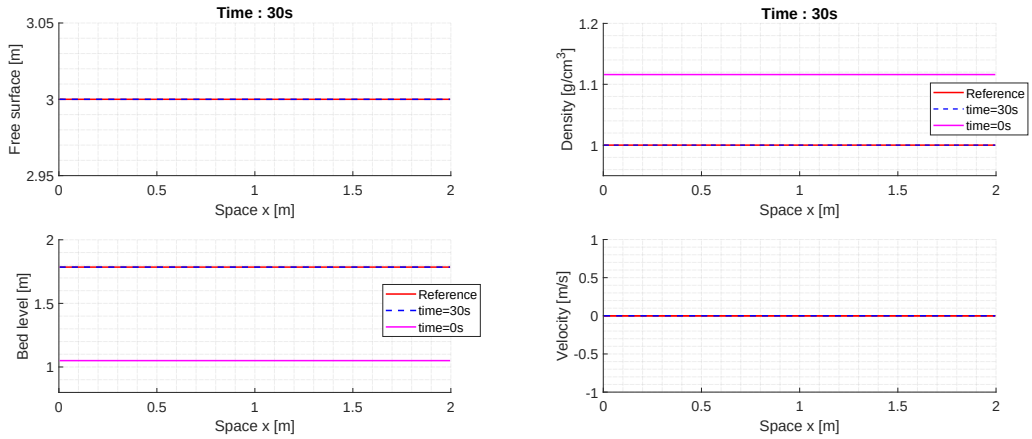

Figure 1: Lake at rest solution with suspended sediment in Section 5.1: $M = 256$ cells, reference solution (red line), $t_{end} = 30$s (blue dashed line), $t_0 = 0$s (magenta line). Free surface and bed level (left), density and velocity (right).

by our numerical outputs, reported in Fig. 1. The solution is computed using the LP-AcTrZ method. We do not report here the results obtained with the other schemes, as they give analogous solution. Finally, remark that we also insert a reference solution found by solving the ODE system (1.8) with a second-order Runge-Kutta method. The reference and LP solutions are analogous as expected.

5.2. Turbidity currents

In this section we want to simulate how the bed elevation evolves in time when imposing turbidity currents into a channel with clear water. Thus, as initial condition we take $h(x, t = 0) = 4$m, $\rho(x, t = 0) = 1$, $z(x, t = 0) = 1$m and $q(x, t = 0) = 0.001$ m^2/s. Moreover, we consider the erosion-deposition source terms together with the friction one but we neglect the solid transport discharge q_z in the Exner equation. Then, we impose $\rho_s = 2.650$ and $r_w = 2.5$ while, for the other parameter values, we use the ones of the previous Section 5.1. Then, for the left boundary condition we do the following:

$$
\begin{aligned}
q(x=0,t) &= \begin{cases} \dfrac{3}{2}\left(1+\sin\left(\dfrac{\pi t}{2}\right)\right), & \text{if} \quad (t \le 20\text{s} \ \vee \ 60\text{s} \le t \le 90\text{s}), \\ q_1(t), & \text{otherwise}, \end{cases} \\
\rho(x=0,t) &= \begin{cases} 1+0.2\max\left(\sin\left(\dfrac{\pi t}{2}\right),0\right), & \text{if} \quad (t \le 20\text{s} \ \vee \ 60\text{s} \le t \le 90\text{s}), \\ \rho_1(t), & \text{otherwise}, \end{cases}
\end{aligned}
\tag{5.1}
$$

where the index 1 indicates the value of the variable in the first cell of the mesh. Otherwise, we ask for transmissive boundary conditions. Then, in Fig. 2, we insert the

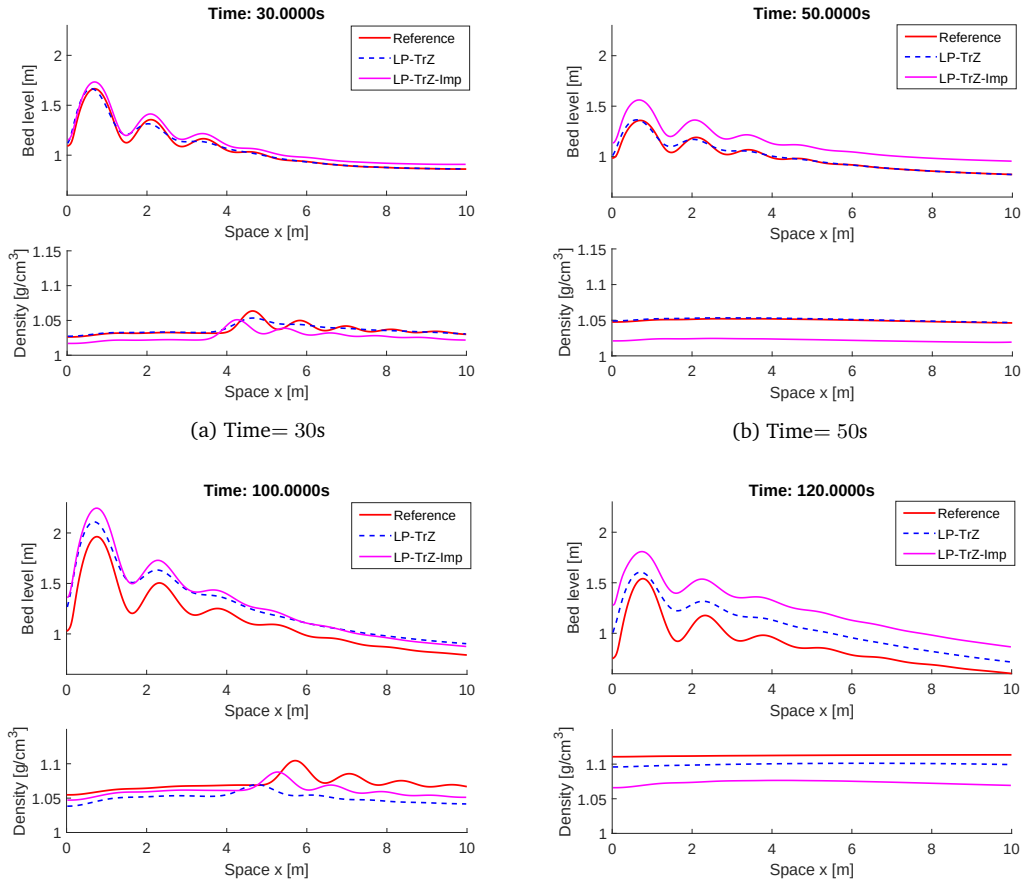

(a) Time= 30s (b) Time= 50s

(c) Time= 100s (d) Time= 120s

Figure 2: Turbidity test in Section 5.2: bed level and density computed with explicit (blue dashed line) and implicit (magenta line) methods with $M = 256$ cells. Reference solution (red line) computed with the explicit scheme and $M = 1024$ cells. Solutions at times $t = 30$s (up-left), $t = 50$s (up-right), $t = 100$s (bottom-left) and $t = 120$s (bottom-right).

bed elevation and density outputs at times $t = 30$s, $t = 50$s, $t = 100$s and $t = 120$s using both explicit and implicit LP-TrZ schemes. Notice that, for the latter, we used a time step based only on the transport CFL condition (4.11). Hence, in this case the implicit time step is at least 14 times larger than the explicit time step, where the latter is about $\Delta t \approx 0.0026$. Notice that we also inserted a reference solution computed with $M = 1024$ cells and the explicit LP-TrZ scheme.

The two schemes give similar results even if some differences can be observed, mainly in the density outputs. This is probably due to the different time steps used for the two simulations. Indeed, differences are reduced if we consider the same time step for the two schemes. Moreover, we verified that the two schemes give analogous solutions when refining the mesh. We stress, anyway, that in this type of test we are mainly interested in understanding how the topography evolves over long periods of

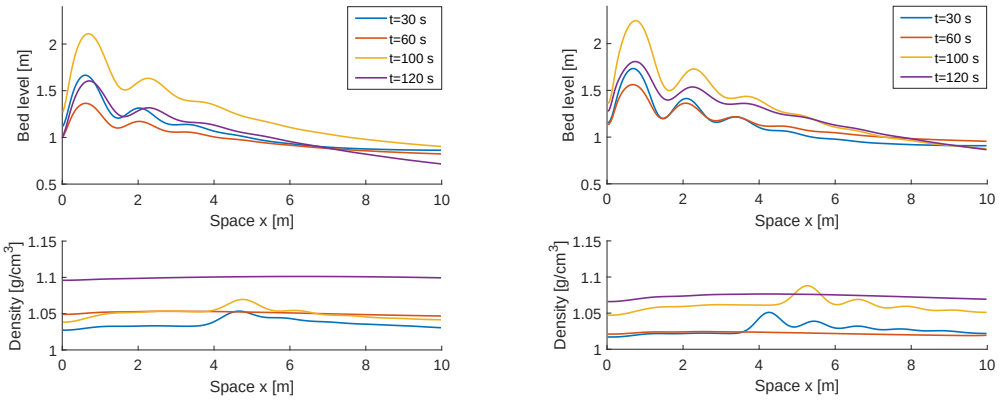

(a) LP-TrZ scheme

(b) LP-TrZ-Imp scheme

Figure 3: Turbidity test in Section 5.2: bed level (up) and density (bottom) computed with explicit (left) and implicit (right) methods and $M = 256$ cells. Solution at times $t = 30$s (blue), $t = 50$s (red), $t = 100$s (yellow) and $t = 120$s (purple).

time rather than density, whose values change several times due to boundary conditions. We can observe that the two schemes give similar pattern for the topography outputs. Moreover, even if the implicit scheme overestimate the topography values, it seems to capture the waveform better, in the sense that the fluctuations are more damped when using the explicit scheme.

Then, to better highlight how the bed elevation changes in time, we insert the outputs at different times in the same figure for the two schemes, see Fig. 3. In particular, we observe that, when inserting the flow with sediment in the channel, the bed elevation increases. On the other hand, when no sediments are imposed, the bed elevation decreases while the density of sediment augments. This is probably due to the fact that here erosion is greater than deposition and, as such, there is an increase of suspended sediments in the water.

Finally, it is interesting to show the errors in norm $\mathbf{L}^1$ and the computational times for both the explicit and implicit schemes, see Table 2. We can conclude that, even if errors are greater when using the implicit scheme, it allows much faster simulation. This explains why the implicit version of the method is useful.

Table 2: CPU time in seconds and errors in norm $\mathbf{L}^1$ for the variables z and ρ computed at times $t = 30$s, $t = 60$s, $t = 100$s and $t = 120$s using LP-TrZ and LP-TrZ-Imp schemes.

Time	Error $\mathbf{L}^1$ of z		Error $\mathbf{L}^1$ of ρ		CPU [s]	
	LP-TrZ	LP-TrZ-Imp	LP-TrZ	LP-TrZ-Imp	LP-TrZ	LP-TrZ-Imp
30s	0.1669	0.5107	0.0216	0.0988	72.4549	4.1708
50s	0.1175	1.4431	0.0103	0.2778	124.0635	6.2851
100s	1.4623	1.6950	0.2042	0.1127	245.2995	15.2274
120s	1.6630	3.4737	0.1265	0.3918	287.0587	17.9937

5.3. Dune evolution test case

For this test case we refer to [4] and we use the following parameters values: $L = 1000$m, $\zeta = 1/(1-0.47)$, Grass formula with $A_g = 1$ and $\mathrm{CFL}_t = 0.5$. Then, the initial conditions (IC) are given by

$$z_{\mathrm{IC}} = \begin{cases} 0.1 + \left(\sin\left(\dfrac{\Pi(x-300)}{200}\right)\right)^2, & \text{if} \quad 300 \le x \le 500, \\ 0.1, & \text{otherwise}, \end{cases}$$

$h_{\mathrm{IC}} = 10 - z_{\mathrm{IC}}$ and $q_{\mathrm{IC}} = 10$. We show the results in Fig. 4, obtained using the LP-TrZ and LP-TrZ-Imp methods. Here the reference solution is computed with $M = 1024$ cells and an implicit-explicit second-order scheme for which we refer to [26]. The numerical solution seems to be in agreement with the one reported in [4]. Let us underline that here we use the implicit-explicit version of the scheme as the dune evolution problem is in general a slow test case. Indeed, the regime is already sub-critical with a Froude number Fr ≈ 0.1. If we set $M = 256$ cells, for the semi-implicit scheme, the time step is about $\Delta t \approx 1.8$s, whereas for the explicit version of the method, the time step is limited to $\Delta t \approx 0.176$s approximately. For the sake of completeness, in Tables 3-4, we show the errors in norm $\mathbf{L}^1$ and the computational times computed with not only the LP-TrZ and LP-TrZ-Imp methods, but also a path-conservative (complete) Riemann Solver (RS) described in [39]. For the variables h and z, we also insert the comparison between the CPU and the errors in log scale in Fig. 5.

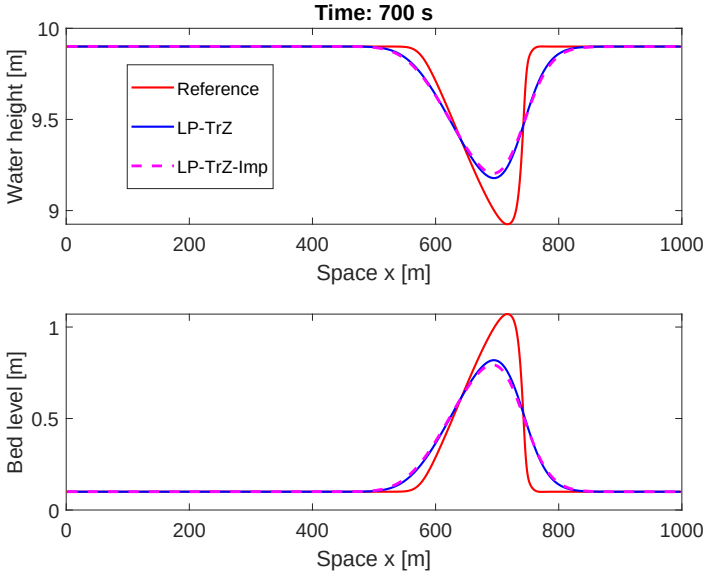

Figure 4: Dune evolution test case in Section 5.3, water height (up) and bed level (bottom). Ending time $t_{end} = 700$s. LP-TrZ (blue line) and LP-TrZ-Imp (magenta dashed line) with $M = 256$ cells and reference solution with $M = 1024$ cells (red line).

Table 3: Errors in norm $\mathbf{L}^1$ of h and hu using LP-TrZ, LP-TrZ-Imp and path-conservative RS methods. Mesh of size $M = (64, 128, 256, 512)$ and space step $\Delta x = (15.625, 7.8125, 3.90625, 1.953125)$.

Mesh	Δx	Error $\mathbf{L}^1$ of h			Error $\mathbf{L}^1$ of hu		
		LP-TrZ	LP-TrZ-Imp	RS	LP-TrZ	LP-TrZ-Imp	RS
64	15.625	74.7145	80.0825	61.1780	30.7352	36.3154	24.8945
128	7.8125	52.8432	57.6222	41.8925	21.6851	26.6577	17.3262
256	3.90625	33.3327	37.0244	25.1158	13.8278	18.3581	10.6593
512	1.953125	19.0688	21.6013	13.6145	8.0738	11.1259	6.0475

Table 4: Errors in norm $\mathbf{L}^1$ of z and computational cost using LP-TrZ, LP-TrZ-Imp and path-conservative RS methods. Mesh of size $M = (64, 128, 256, 512)$ and space step $\Delta x = (15.625, 7.8125, 3.90625, 1.953125)$.

Mesh	Δx	Error $\mathbf{L}^1$ of z			CPU [s]		
		LP-TrZ	LP-TrZ-Imp	RS	LP-TrZ	LP-TrZ-Imp	RS
64	15.625	74.2672	79.8077	60.9452	1.2478	0.1833	1.4491
128	7.8125	52.6857	57.4422	41.7470	4.2625	0.4024	4.7655
256	3.90625	33.2159	36.8888	25.0112	15.4166	1.9843	20.0654
512	1.953125	18.9822	21.4826	13.5388	61.2181	9.5504	183.2754

We highlight that, for this test, we considered a long channel ($L = 1000$m) with relatively coarse meshes and large space steps Δx. As a consequence, also the errors appear to be big, which is normal as we assume them to be of the same order of Δx. Then, we observe that the errors of the LP explicit scheme are a bit smaller than the LP implicit ones when using the same mesh values. This is expected as the implicit method is more diffusive than the explicit one. On the other hand, it is immediately

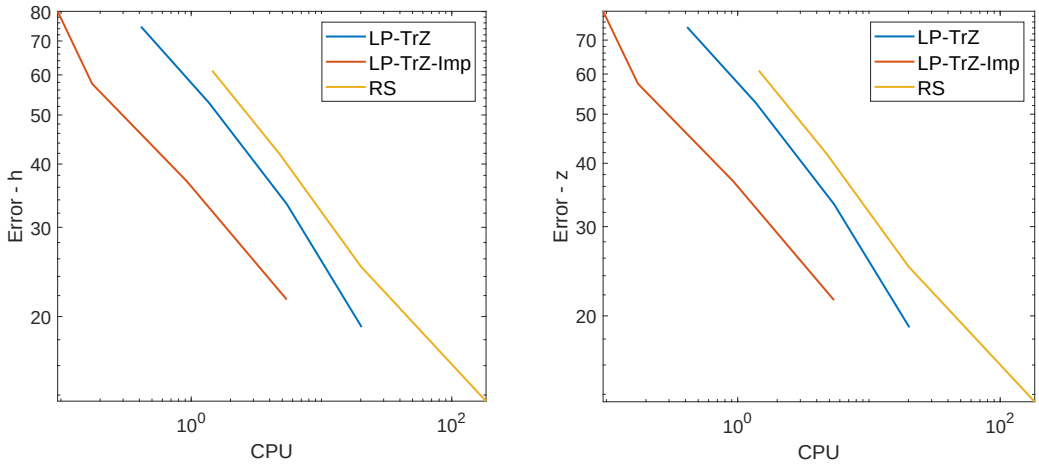

Figure 5: Dune evolution test case in Section 5.3: CPU against error in norm $\mathbf{L}^1$ for the variables h (left) and z (right). Mesh of size $M = (64, 128, 256, 512)$. LP-TrZ (blue line), LP-TrZ-Imp (red line) and path-conservative RS (yellow line) schemes.

evident that the LP-TrZ-Imp scheme is much faster than its explicit version. Therefore, it is clear that the LP-TrZ method is more accurate, but the difference on CPU time when compared to the implicit scheme makes the LP-TrZ-Imp method a very good alternative for long time simulations. This fact is made even clearer by Fig. 5, where we observe that the line for the LP-TrZ-Imp scheme is always under the LP-TrZ one, confirming our previous statement. Then, let us compare the LP schemes with a more classical method: a first-order complete Riemann solver. It appears clear that, even if the RS is more accurate than both the LP methods for a fixed mesh, it also has a greater computational cost. This is due to the smaller time steps which are used to advance in time. To make a comparison, for $M = 256$ and $\mathrm{CFL} = 0.45$, we approximately need to impose $\Delta t \approx 0.118$ for the RS method. This confirms that implicit LP-methods are indeed competitive compared to other conventional schemes when working in subsonic regimes, in which long ending times are required.

Moreover, here we have taken $A_g = 1$, meaning that the interaction between the fluid and the sediments of the bottom is strong. In this way we are able to see in a relative short time substantial changes in the bed elevation. However, if we consider a weaker interaction, for instance $A_g < 0.1$, the evolution of the bottom height is slower and we need a greater ending time to be able to see significant changes in z, hence the usefulness of the implicit-explicit version of the method. Finally, we underline that if we are in a low Froude number regime ($\mathrm{Fr} < 10^{-2}$), the CFL condition for the acoustic time step is even more limited and difference in value between the acoustic and transport time steps could be more remarkable.

Finally, for the sake of completeness, in Table 5 we insert the empirical convergence rates for the LP-TrZ and LP-TrZ-Imp schemes in order to show that their order of accuracy tends to one.

Table 5: Empirical convergence rates in norm $\mathbf{L}^1$ of h, hu, z using LP-TrZ and LP-TrZ-Imp methods. Mesh of size $M = (64, 128, 256, 512)$.

Mesh	$\mathcal{O}(\mathbf{L}^1)$ of h		$\mathcal{O}(\mathbf{L}^1)$ of hu		$\mathcal{O}(\mathbf{L}^1)$ of z	
	LP-TrZ	LP-TrZ-Imp	LP-TrZ	LP-TrZ-Imp	LP-TrZ	LP-TrZ-Imp
64	–	–	–	–	–	–
128	0.4997	0.4749	0.5032	0.4460	0.4953	0.4744
256	0.6648	0.6381	0.6491	0.5381	0.6655	0.6389
512	0.8057	0.7774	0.7763	0.7225	0.8072	0.7800

5.4. Dam break problems

Here we present two different dam break problems for which the experimental results are available. The experiments are selected from [32, 53]. We consider the MPM formulation (1.3) for q_z and describe the parameters values in Table 6. We also take $M = 500$ cells. Let us remark that for these dam break problems, we need to use a smaller time step value for the LP-TrZ method in order to avoid unphysical oscillations.

Table 6: Parameters values for dam break problems in Section 5.4, two different experiments.

Experiment	h_L [m]	h_R [m]	L [m]	d [mm]	ρ_s [g cm^{-3}]	μ_f [s m$^{-1/3}$]	θ_c^*	r_w
1	0.1	0	2.5	3.2	1.540	0.02	0.045	1
2	0.35	0	6	3.9	1.580	0.0165	0.047	2.5

Experiment 1. This experiment has been carried on at the Université Catholique de Louvain and is in particular described in [32]. We report the LP-AcTrZ and LP-TrZ results for this first dam break experiment in Fig. 6. In particular, on the left we insert the LP-AcTrZ solution against the experimental results, while we compare the two LP-AcTrZ and LP-TrZ methods on the right. We consider three different ending times, namely $t_{end} = 5t_0, 7.5t_0, 10t_0$ s with $t_0 = \sqrt{gh_0} \approx 0.101$. In general, the numerical outputs seem to be in agreement with the ones reported in [39] and they are also close to the experimental solution. We can also observe that the two LP-AcTrZ and LP-TrZ methods give similar results, even if the LP-TrZ method is less diffusive, see again Fig. 6. Finally, we do not report here the implicit LP-TrZ outputs as they are analogous to the ones of the explicit version of the scheme.

Experiment 2. The second dam break experiment was selected from [53]. In Fig. 7, once again we show the LP-AcTrZ and LP-TrZ outputs for the second dam break problem. Analogous comments to what we have made for the first experiment may be said: our numerical solution correctly describe the solution in the sense that it is close to the experimental one. The position of the front is correct as well. Finally, the LP-TrZ is slightly less diffusive than the LP-AcTrZ one but it may require the use of a smaller CFL number to avoid possible spurious oscillations.

Remark 5.1. Let us observe that for these two dam break problems, the regime is supercritical. As such, to exploit the implicit version of the method does not lead to an actual improvement of the numerical simulation in the sense that CPU times are not necessarily better. On the other hand, while the first-order numerical scheme LP-TrZ does not produce spurious oscillations, its second (or higher) order extension could, see [17]. Hence, the usefulness of the LP-AcTrZ method, which is more stable.

6. Conclusion and perspectives

In this work, we have presented both explicit and implicit-explicit well-balanced Lagrange-projection schemes applied to the shallow water system with moving topography and variable density of the mixture water-sediment. In particular, we assumed that sediments could move along the bottom (bed-load) or being finer fraction that could be carried in suspension into the water or be deposited on the bed.

Since sediment transport is generally a slow process, which requires long-in-time simulation in order to see appreciable changes in the bed elevation, implicit-explicit method can be very useful. We considered academic problems to show that the implicit-

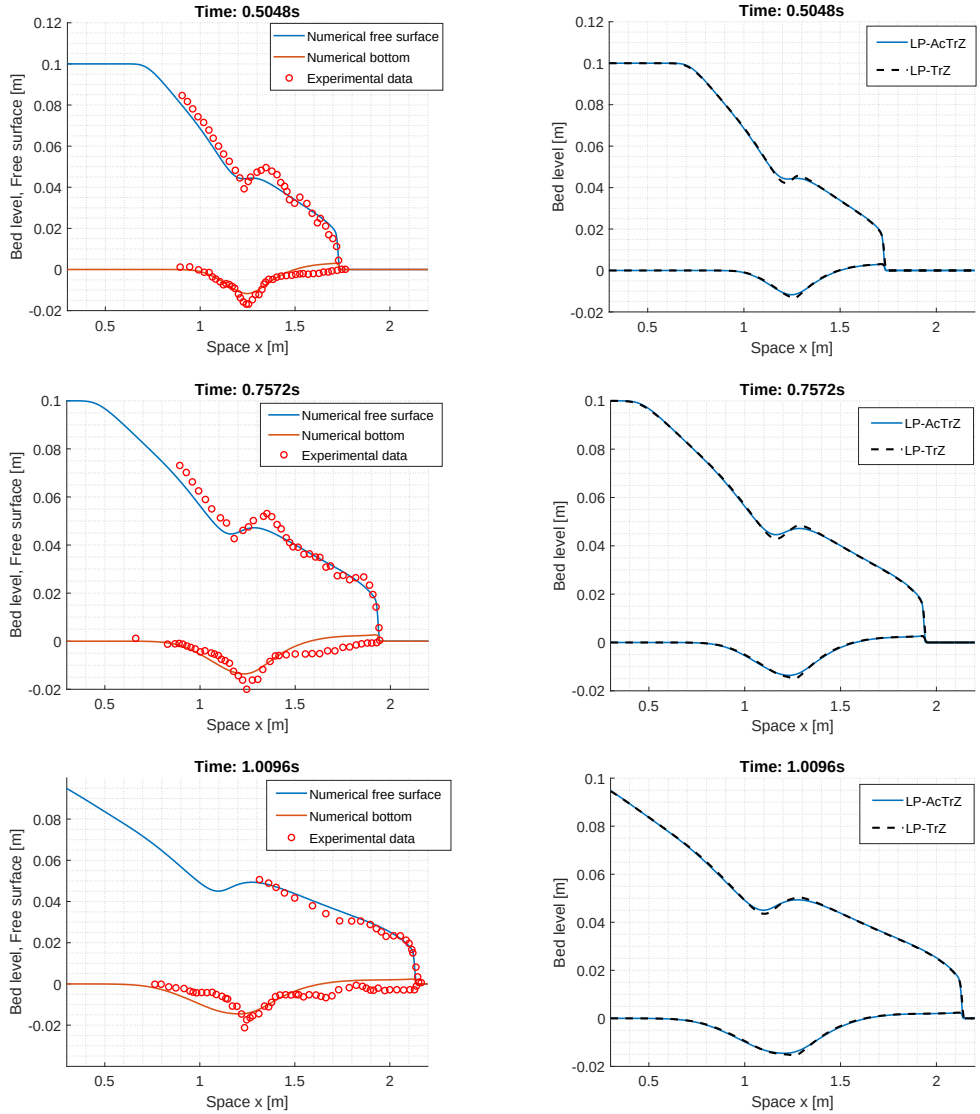

Figure 6: Dam break problem, Experiment 1, Section 5.4: free surface and bed level, $M = 500$ cells. Ending time $t_{end} = 5t_0$s (up), $t_{end} = 7.5t_0$s (middle), $t_{end} = 10t_0$s (bottom). On the left, LP-AcTrZ free surface (blue line), LP-AcTrZ bottom (red line) and experimental values (red symbol). On the right, LP-AcTrZ (continuous blue line) and LP-TrZ (black dashed line) numerical methods.

explicit version of the Lagrange-projection numerical scheme allows very fast simulations, especially when we are in subsonic or low-Froude number regimes. Indeed, the LP approach entails a decomposition of the acoustic and transport waves of the model leading to the possibility of implicitly approximating only the acoustic equations. As a consequence, the CFL condition on the time step can be based only on the transport waves. Finally, we also provided comparison between experimental and numerical results.

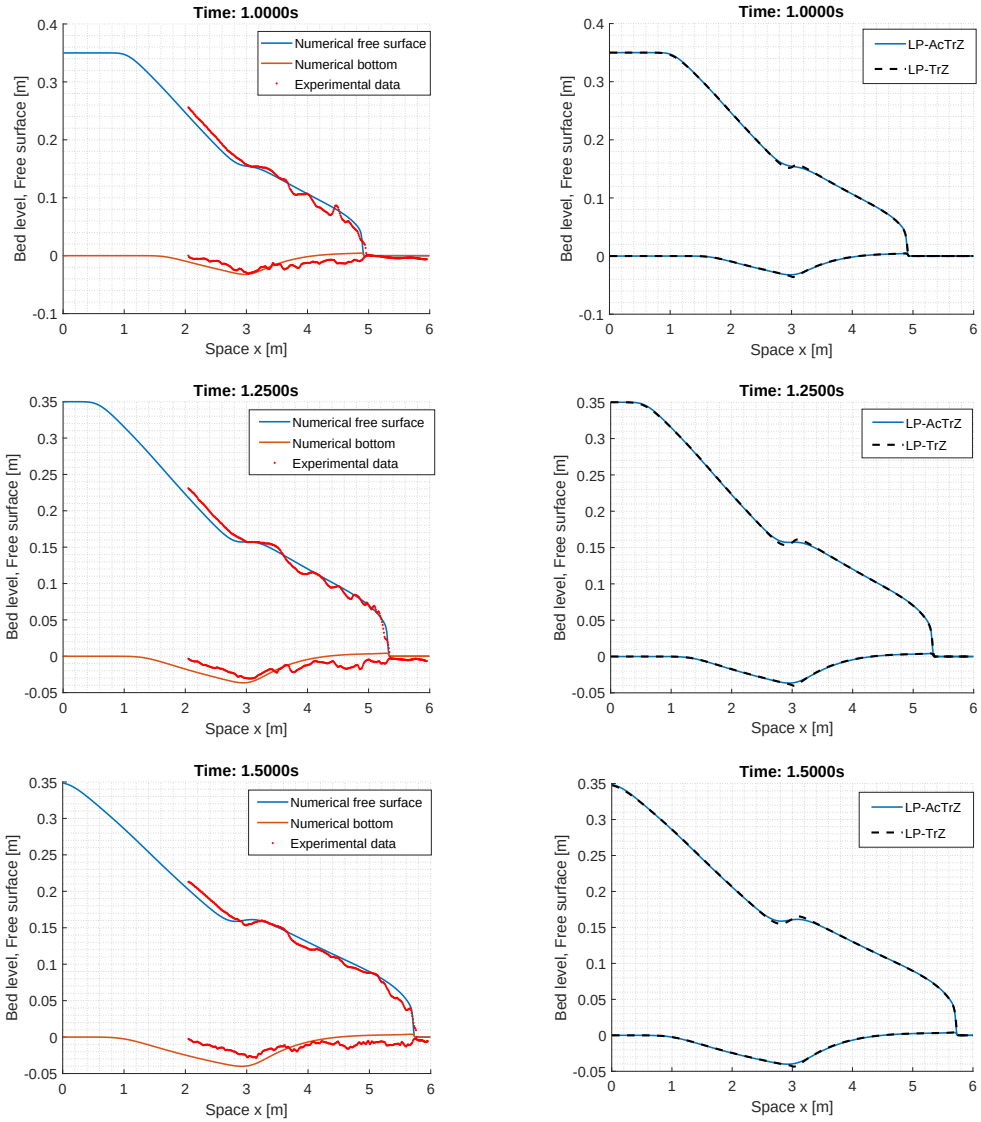

Figure 7: Dam break problem, Experiment 2, Section 5.4: free surface and bed level, $M = 500$ cells. Ending time $t_{end} = 1$s (up), $t_{end} = 1.25$s (middle), $t_{end} = 1.5$s (bottom). On the left, LP-AcTrZ free surface (blue line), LP-AcTrZ bottom (red line) and experimental values (red symbol). On the right, LP-AcTrZ (continuous blue line) and LP-TrZ (black dashed line) numerical methods.

We note that two explicit LP schemes have been described, which differ only in the approximation of the bed elevation z, namely the LP-TrZ and the LP-AcTrZ. Indeed, while the former is easier, the latter proved to be more stable in situations in which we could expect unphysical oscillation in the numerical outputs of fully decoupled methods.

Improvements could be related to the design and implementation of high order extension of implicit-explicit well-balanced Lagrange-projection schemes.

Finally, we want to highlight that the numerical method presented here could be applied in situations with or without bedload transport. Moreover, it can be extended to more sophisticated models like multi-layer or multi-phase flows.

Appendix A. Linear system for the implicit acoustic approximation

In this section we briefly show how to write the implicit version of the numerical scheme which approximates the Exner equation directly in the transport step. For this purpose, we reformulate the third and fourth equations of system (4.4) as the following linear system $A\overrightarrow{X} = \overrightarrow{b}$, where

$$\overrightarrow{X} = \begin{pmatrix} u_1^{n+} \\ \Pi_1^{n+} \\ \vdots \\ u_j^{n+} \\ \Pi_j^{n+} \\ \vdots \\ u_M^{n+} \\ \Pi_M^{n+} \end{pmatrix}, \quad \overrightarrow{b} = \begin{pmatrix} u_1^n + \dfrac{\Delta t}{\Delta m_1} s_1^n \\ \Pi_1^n - a_{3/2}^2 \dfrac{\Delta t}{2\Delta m_1} \left(\dfrac{s_{3/2}^n}{a_{3/2}} - \dfrac{s_{1/2}^n}{a_{1/2}} \right) \\ \vdots \\ u_j^n + \dfrac{\Delta t}{\Delta m_j} s_j^n \\ \Pi_j^n - a_{j+1/2}^2 \dfrac{\Delta t}{2\Delta m_j} \left(\dfrac{s_{j+1/2}^n}{a_{j+1/2}} - \dfrac{s_{j-1/2}^n}{a_{j-1/2}} \right) \\ \vdots \\ u_M^n + \dfrac{\Delta t}{\Delta m_M} s_M^n \\ \Pi_M^n - a_{M+1/2}^2 \dfrac{\Delta t}{2\Delta m_M} \left(\dfrac{s_{M+1/2}^n}{a_{M+1/2}} - \dfrac{s_{M-1/2}^n}{a_{M-1/2}} \right) \end{pmatrix} \tag{A.1}$$

and

$$A = \begin{pmatrix} c_1 & f_1 & d_1 & g_1 & 0 & \dots & \dots & \dots & \dots & 0 \\ \tilde{c}_1 & \tilde{f}_1 & \tilde{d}_1 & \tilde{g}_1 & 0 & \dots & \dots & \dots & \dots & 0 \\ b_2 & e_2 & c_2 & f_2 & d_2 & g_2 & 0 & \dots & \dots & 0 \\ \tilde{b}_2 & \tilde{e}_2 & \tilde{c}_2 & \tilde{f}_2 & \tilde{d}_2 & \tilde{g}_2 & 0 & \dots & \dots & 0 \\ 0 & \ddots & \ddots & \ddots & \ddots & \ddots & \ddots & 0 & \dots & 0 \\ \dots & 0 & b_j & e_j & c_j & f_j & d_j & g_j & 0 & \dots \\ \dots & 0 & \tilde{b}_j & \tilde{e}_j & \tilde{c}_j & \tilde{f}_j & \tilde{d}_j & \tilde{g}_j & 0 & \dots \\ 0 & \dots & 0 & \ddots & \ddots & \ddots & \ddots & \ddots & \ddots & 0 \\ 0 & \dots & \dots & 0 & \ddots & \ddots & \ddots & \ddots & \ddots & \ddots \\ 0 & \dots & \dots & \dots & 0 & \ddots & \ddots & \ddots & \ddots & \ddots \\ 0 & \dots & \dots & \dots & \dots & 0 & b_M & e_M & c_M & f_M \\ 0 & \dots & \dots & \dots & \dots & 0 & \tilde{b}_M & \tilde{e}_M & \tilde{c}_M & \tilde{f}_M \end{pmatrix} \tag{A.2}$$

with

$$
\begin{aligned}
b_j &= -\frac{\Delta t}{2\Delta m_j} a^n_{j-1/2}, & c_j &= 1 + \frac{\Delta t}{\Delta m_j}\left(\frac{a^n_{j+1/2} + a^n_{j-1/2}}{2}\right),\\
d_j &= -\frac{\Delta t}{2\Delta m_j} a^n_{j+1/2}, & e_j &= -\frac{\Delta t}{2\Delta m_j}, \qquad f_j = 0,\\
g_j &= +\frac{\Delta t}{2\Delta m_j}, & \tilde{b}_j &= -\frac{\Delta t}{2\Delta m_j}\left(a^n_{j+1/2}\right)^2, \quad \tilde{c}_j = 0,\\
\tilde{d}_j &= +\frac{\Delta t}{2\Delta m_j}\left(a^n_{j+1/2}\right)^2, & \tilde{e}_j &= -\frac{(a^n_{j+1/2})^2 \Delta t}{2a^n_{j-1/2}\Delta m_j},\\
\tilde{f}_j &= 1 + \frac{(a^n_{j+1/2})^2 \Delta t}{2\Delta m_j}\left(\frac{1}{a^n_{j+1/2}} + \frac{1}{a^n_{j-1/2}}\right), & \tilde{g}_j &= -\frac{(a^n_{j+1/2})^2 \Delta t}{2a^n_{j+1/2}\Delta m_j}.
\end{aligned}
$$

By the index 1 and M we indicate the value of the variable in the first and last cell respectively, where M is the number of cells. Finally, it is clear that the first and last line of the system should be modified according to the considered boundary condition.

Then, once u^{n+} and Π^{n+} have been recovered, it is straightforward to update the variables Lh^{n+}, $Lh\rho^{n+}$ and $Lh\rho u^{n+}$ by considering the Lagrangian approximation (4.1) with star values at time t^{n+}.

Acknowledgments

A. Del Grosso research has been supported by a grant from Région Île-de-France. M.J. Castro research has been partially supported by the Spanish Government and FEDER through the coordinated Research project RTI2018-096064-B-C1 and PID2022-137637NB-C21, the Junta de Andalucía research project P18-RT-3163, the Junta de Andalucia-FEDER-University of Málaga research project UMA18-FEDERJA-163 and the University of Málaga. T. Morales de Luna has been partially supported by the Spanish Government and FEDER through the coordinated Research project RTI2018-096064-B-C2 and PID2022-137637NB-C21, and by the the Junta de Andalucía research project PROYEXCEL-00525.

References

[1] E. Audusse, C. Berthon, C. Chalons, O. Delestre, N. Goutal, M. Jodeau, J. Sainte-Marie, J. Giesselmann, and G. Sadaka, *Sediment transport modelling: Relaxation schemes for Saint-Venant-Exner and three layer models*, ESAIM: Proceedings 38 (2012), 78–98.

[2] E. Audusse, F. Bouchut, M.-O. Bristeau, R. Klein, and B. Perthame, *A fast and stable well-balanced scheme with hydrostatic reconstruction for shallow water flows*, SIAM J. Sci. Comput. 25(6) (2004), 2050–2065.

[3] E. AUDUSSE, C. CHALONS, P. UNG, *A simple three-wave approximate Riemann solver for the Saint-Venant-Exner equations*, Internat. J. Numer. Methods Fluids 87 (2018), 508–528.
[4] E. AUDUSSE, O. DELESTRE, M. LE, M. MASSON-FAUCHIER, P. NAVARO, AND R. SERRA, *Parallelization of a relaxation scheme modelling the bedload transport of sediments in shallow water flow*, ESAIM: Proceedings 43 (2013), 80–94.
[5] M. BAUDIN, C. BERTHON, F. COQUEL, M. ROLAND, AND Q.-H. TRAN, *A relaxation method for two-phase flow models with hydrodynamic closure law*, Numerische Mathematik 99 (2005), 411–440.
[6] C. BERTHON, S. CORDIER, O. DELESTRE, AND M. H. LE, *An analytical solution of the shallow water system coupled to the Exner equation*, Comptes Rendus Mathematique 350 (2012), 183–186.
[7] L. BONAVENTURA, E. D. FERNÁNDEZ-NIETO, J. GARRES-DÍAZ, AND G. NARBONA-REINA, *Multilayer shallow water models with locally variable number of layers and semi-implicit time discretization*, J. Comput. Phys. 364 (2018), 209–234.
[8] F. BOUCHUT, *Nonlinear Stability of Finite Volume Methods for Hyperbolic Conservation Laws and Well-Balanced Schemes for Sources*, Birkhäuser, 2004.
[9] R. BRIGANTI, N. DODD, D. KELLY, AND D. POKRAJAC, *An efficient and flexible solver for the simulation of the morphodynamics of fast evolving flows on coarse sediment beaches*, Internat. J. Numer. Methods Fluids 69 (2011), 859–877.
[10] V. CALEFFI, A. VALIANI, AND A. BERNINI, *High-order balanced CWENO scheme for movable bed shallow water equations*, Adv Water Resour 30 (2007), 730–741.
[11] M. CASTRO, E. FERNÁNDEZ-NIETO, AND A. FERREIRO, *Sediment transport models in shallow water equations and numerical approach by high order finite volume methods*, Comput. & Fluids 37 (2008), 299–316.
[12] M. J. CASTRO DÍAZ, C. CHALONS, AND T. MORALES DE LUNA, *A fully well-balanced Lagrange-projection-type scheme for the shallow-water equations*, SIAM J. Numer. Anal. 56 (2018), 3071–3098.
[13] V. CASULLI, *Semi-implicit finite difference methods for the two-dimensional shallow water equations*, J. Comput. Phys. 86 (1990), 56–74.
[14] V. CASULLI, *Numerical simulation of three-dimensional free surface flow in isopycnal coordinates*, Internat. J. Numer. Methods Fluids 25 (1997), 645–658.
[15] V. CASULLI AND E. CATTANI, *Stability, accuracy and efficiency of a semi-implicit method for three-dimensional shallow water flow*, Comput. Math. Appl. 27 (1994), 99–112.
[16] V. CASULLI AND P. ZANOLLI, *Semi-implicit numerical modeling of nonhydrostatic free-surface flows for environmental problems*, Mathematical and Computer Modelling 36 (2002), 1131–1149.
[17] C. CHALONS AND A. DEL GROSSO, *Exploring different possibilities for second-order well-balanced Lagrange-projection numerical schemes applied to shallow water exner equations*, Internat. J. Numer. Methods Fluids 94 (2022), 505–535.
[18] C. CHALONS AND A. DEL GROSSO, *A second-order well-balanced Lagrange-projection numerical scheme for shallow water Exner equations in 1d and 2d*, Commun. Math. Sci. 20 (2022), 1839–1873.
[19] C. CHALONS, M. GIRARDIN, AND S. KOKH, *Large time step and asymptotic preserving numerical schemes for the gas dynamics equations with source terms*, SIAM J. Sci. Comput. 35 (2013), A2874–A2902.
[20] C. CHALONS, M. GIRARDIN, AND S. KOKH, *An all-regime Lagrange-projection like scheme for the gas dynamics equations on unstructured meshes*, Commun. Comput. Phys. 20 (2016), 188–233.

[21] C. CHALONS, M. GIRARDIN, AND S. KOKH, *An all-regime Lagrange-projection like scheme for 2d homogeneous models for two-phase flows on unstructured meshes*, J. Comput. Phys. 335 (2017), 885–904.

[22] C. CHALONS, P. KESTENER, S. KOKH, AND M. STAUFFERT, *A large time-step and well-balanced Lagrange-projection type scheme for the shallow water equations*, Commun. Math. Sci. 15 (2017), 765–788.

[23] F. COQUEL, E. GODLEWSKI, B. PERTHAME, A. IN, AND P. RASCLE, *Some new Godunov and relaxation methods for two-phase flow problems*. In: Godunov Methods, E. F. Toro (Eds), Springer, (2001), 179-–188.

[24] S. CORDIER, M. LE, AND T. MORALES DE LUNA, *Bedload transport in shallow water models: Why splitting (may) fail, how hyperbolicity (can) help*, Adv Water Resour 34 (2011), 980–989.

[25] L. COZZOLINO, L. CIMORELLI, C. COVELLI, R. DELLA MORTE, AND D. PIANESE, *Novel numerical approach for 1d variable density shallow flows over uneven rigid and erodible beds*, J. Hydraul. Eng. 140 (2014), 254–268.

[26] A. DEL GROSSO, *Numerical Simulation of Geophysical Flows Using High-Order and Well-Balanced Lagrange-Projection Methods*, PhD Thesis, 2022.

[27] A. DEL GROSSO AND C. CHALONS, *Second-order well balanced Lagrange-projection schemes for blood flow equations*, Calcolo, 58 (2021).

[28] F. DUBOC, C. ENAUX, S. JAOUEN, H. JOURDREN, AND M. WOLFF, *High-order dimensionally split Lagrange-remap schemes for compressible hydrodynamics*, Comptes Rendus Mathematique 348 (2010), 105–110.

[29] H. A. EINSTEIN, *The bed load function for sediment transportation in open channel flows*, Technical Bulletin 1026, 1950.

[30] F. M. EXNER, *Über die wechselwirkung zwischen wasser und geschiebe in flüsen*, Akad. Wiss. Wien Math. Naturwiss, Klasse, 134 (1925), 165–2014.

[31] E. D. FERNÁNDEZ-NIETO, T. MORALES DE LUNA, G. NARBONA-REINA, AND J. D. ZABSONRÉ, *Formal deduction of the Saint-Venant-Exner model including arbitrarily sloping sediment beds and associated energy*, Esaim Math Model Numer Anal 51 (2017), 115–145.

[32] L. FRACCARROLLO AND H. CAPART, *Riemann wave description of erosional dam-break flows*, J. Fluid Mech. 461 (2002), 183–238.

[33] G. GALLICE, *Positive and entropy stable Godunov-type schemes for gas dynamics and MHD equations in Lagrangian or Eulerian coordinates*, Numerische Mathematik 94 (2002), 673–713.

[34] G. GALLICE, *Solveurs simples positifs et entropiques pour les systèmes hyperboliques avec terme source*, Comptes Rendus Mathematique 334 (2002), 713–716.

[35] J. GARRES-DÍAZ AND L. BONAVENTURA, *Flexible and efficient discretizations of multilayer models with variable density*, Appl. Math. Comput. 402 (2021), 126097.

[36] J. GARRES-DÍAZ, E. FERNÁNDEZ-NIETO, AND G. NARBONA-REINA, *A semi-implicit approach for sediment transport models with gravitational effects*, Appl. Math. Comput. 421 (2022), 126938.

[37] I. GÓMEZ-BUENO, M. J. CASTRO, C. PARÉS, AND G. RUSSO, *Collocation methods for high-order well-balanced methods for systems of balance laws*, Mathematics 9(15) (2021), 1799.

[38] C. GOÑI, D. CELI, AND F. CONCHA, *Determination of the volumetric solids fraction of saturated polydisperse ore tailing sediments*, Powder Technol. 305 (2017), 528–537.

[39] J. GONZALEZ, M. CASTRO, AND T. MORALES DE LUNA, *A robust model for rapidly varying flows over movable bottom with suspended and bedload transport: Modelling and numerical approach*, Adv Water Resour 140 (2020), 103575.

[40] A. GRASS, *Sediment transport by waves and currents*, SERC London Cent. Mar. Technol, Report No. FL29 (1981).
[41] S. M. KHAN, J. IMRAN, S. BRADFORD, AND J. SYVITSKI, *Numerical modeling of hyperpycnal plume*, Mar. Geol., 222-223 (2005), 193–211.
[42] S. KOMURA AND B. R. COLBY, *Discussion of "Sediment transportation mechanics: Introduction and properties of sediment, progress report by the task committee on preparation of sedimentation manual of the committee on sedimentation of the hydraulics division"*, J. Hydraul. Div. 89(1) (1963), 263–268.
[43] Y. KUBO, *Experimental and numerical study of topographic effects on deposition from two-dimensional, particle-driven density currents*, Sediment. Geol. 164 (2004), 311–326.
[44] Y. KUBO AND T. NAKAJIMA, *Laboratory experiments and numerical simulation of sediment-wave formation by turbidity currents*, Mar. Geol. 192 (2002), 105–121.
[45] X. MENG, T.-T. P. HOANG, Z. WANG, AND L. JU, *Localized exponential time differencing method for shallow water equations: Algorithms and numerical study*, Commun. Comput. Phys. 29(1) (2021), 80–110.
[46] E. MEYER-PETER AND R. MÜLLER, *Formulas for bed-load transport*. In: IAHSR 2nd Meeting, Sweden, (1948), 1–26.
[47] Z. MIN, H. WEIZHANG, AND J. QIU, *A well-balanced positivity-preserving quasi-Lagrange moving mesh DG method for the shallow water equations*, Commun. Comput. Phys. 31 (2021), 94–130.
[48] T. MORALES DE LUNA, M. J. CASTRO DÍAZ, AND C. CHALONS, *High-order fully well-balanced Lagrange-projection scheme for shallow water*, Commun. Math. Sci. 18 (2020), 781–807.
[49] T. MORALES DE LUNA, M. J. CASTRO DÍAZ, C. PARÉS MADROÑAL, AND E. D. FERNÁNDEZ NIETO, *On a shallow water model for the simulation of turbidity currents*, Commun. Comput. Phys. 6 (2009), 848–882.
[50] J. MURILLO AND P. GARCÍA-NAVARRO, *An exner-based coupled model for two-dimensional transient flow over erodible bed*, J. Comput. Phys. 229 (2010), 8704–8732.
[51] G. PARKER, Y. FUKUSHIMA, AND H. M. PANTIN, *Self-accelerating turbidity currents*, J. Fluid Mech. 171 (1986), 145–181.
[52] L. RIJN, *Sediment transport, Part I: Bed load transport*, Journal of Hydraulic Engineering, 110 (1984), 1431–1456.
[53] B. SPINEWINE AND Y. ZECH, *Small-scale laboratory dam-break waves on movable beds*, J. Hydraul. Res. 45 (2007), 73–86.
[54] D. SUBHASISH, *Fluvial Hydrodynamics, Hydrodynamic and Sediment Transport Phenomena*, GeoPlanet: Earth and Planetary Sciences, Springer-Verlag, 2014.
[55] I. SULICIU, *On the thermodynamics of rate-type fluids and phase transitions. i. rate-type fluids*, Internat. J. Engrg. Sci. 36 (1998), 921–947.
[56] W. WU AND S. S. Y. WANG, *Formulas for sediment porosity and settling velocity*, J. Hydraul. Eng. 132 (2006), 858–862.